Oil & Natural Gas Technology

DOE Award No.: DE-FE0024297

Quarterly Research Performance

Progress Report (Period Ending 12/30/2018)

Marcellus Shale Energy and Environment Laboratory (MSEEL)

Project Period (October 1, 2014 – September 30, 2019)

Submitted by:
Samuel Taylor

Signature

West Virginia University Research Corporation
DUN's Number: 191510239
886 Chestnut Ridge Road,
PO Box 6845, Morgantown WV, 26505
Tim.Carr@mail.wvu.edu
304-293-9660

Prepared for:
United States Department of Energy
National Energy Technology Laboratory

1/31/2019

U.S. DEPARTMENT OF ENERGY | NATIONAL ENERGY TECHNOLOGY LABORATORY

Office of Fossil Energy

Executive Summary
Quarterly Progress Report

October 1 – December 30, 2018

The objective of the Marcellus Shale Energy and Environment Laboratory (MSEEL) is to provide a long-term field site to develop and validate new knowledge and technology to improve recovery efficiency and minimize environmental implications of unconventional resource development.

This quarter work focused on reservoir simulation and attempting to understand effects of well spacing and the how preexisting factures affect completion and production efficiencies.

We developed an improved history match that incorporates the unconventional fracture model and demonstrated how knowledge of geomechanical properties could be used this knowledge to increase production, efficiently space laterals and reduce cost. Manuscripts has been accepted for presentation to the Society of Petroleum Engineers Annual Meeting and for URTeC on these subjects.

A provisional patent application for analysis of fiber-optic data is moving forward and we have demonstrated to several companies.

Plans developed for MSEEL Phase 3 were presented to the technical advisory group and to DOE. Costs for various scenarios were evaluated. The Boggess pad consisting of six wells was selected.

Project Performance

This report summarizes the activities of Cooperative Agreement DE-FE0024297 (Marcellus Shale Energy and Environment Laboratory – MSEEL) with the West Virginia University Research Corporation (WVURC) during the first quarter of FY2019 (October 1 through December 30, 2018).

This report outlines the approach taken, including specific actions by subtopic. If there was no identified activity during the reporting period, the appropriate section is included but without additional information.

A summary of major lessons learned to this point of the project are provided as bullet points and will be added to as research is completed. New lessons listed below are:

Phase 3 Plans

A phase 3 of MSEEL was presented to the Technical Advisory Group for their input and approval in December. MSEEL Phase 3 provides a unique opportunity and platform to test technologies and develop an integrated reservoir model for six 10,000+ foot horizontal Marcellus Shale wells off a single pad (Boggess) very near the initial MIP pad (Figure 1.1). The proposed phase of the project will be able to test multiple technologies and engineered completions (fracture stimulation) over multiple wells and 100's of stages. The plan as proposed will have at least one well with permanent fiber optic (FO) cable installed that will provide digital acoustic sensing (DAS) during stimulation and distributed temperature sensing (DTS) during stimulation and long-term production monitoring along the lateral (Boggess 5H). Two deployable FO systems are also proposed (Boggess 3H and 9H). This will permit evaluation of stimulation effectiveness in near real-time and the 100's of terabytes of data to evaluate and model the reservoir across each individual stage, and at individual clusters within stages for 3 wells. The deployable fiber in parallel wells (skipping one adjacent) will allow excellent microseismic imaging, recognition and evaluation of long-period long-duration events in the test well. We will also be able to monitor adjacent wells to the test well during stimulation. We have developed techniques to use the permanent DAS and DTS monitoring in the 5H to determine production rates and changes at the stage level through the life of the well.

The cored and logged vertical pilot well will allow development of a high-resolution geomechanical model (stratigraphy) to type each 6 inches of the Marcellus. Logging while drilling (LWD) logs in each of the six laterals provide similar geomechanical logs and image logs to geomechanically type each foot of the laterals as the horizontal laterals move stratigraphically up and down through the Marcellus. This approach permits direct coupling and evaluation of cost-effective LWD technologies to the relatively high-cost permanent FO data and the basis for engineering stages in all wells.

The plan is to undertake at least two of the laterals with the standard industrial geometrical completion practice (identical 200 feet stages with identical number of clusters in each stage). These will be the control wells. We will use the LWD and permanent FO in the one well (extremely large big data) and the LWD and microseismic only (relatively "thin" data) in the other wells to engineer stage and cluster spacing. Coupled with production data from all the wells including the control wells, this provides the basis to evaluate the reservoir through modeling and direct monitoring to develop a first ever, publicly available, multi-well unconventional fractured reservoir simulation.

MSEEL 2 will be able to compare across the six wells and with the MIP pad (MSEEL 1) and use these data to form the basis for robust big data modeling. MSEEL 1 generated almost 10

terabytes of data and created approaches and capabilities to handle and process big data sets (i.e., volume, variety, velocity and veracity) from a single well to address the spacing between laterals and stage length, the importance of modeling at multiple scales from nanopores in kerogen to healed fractures spaced along the lateral, and the approaches to engineering stage and cluster design and stimulation processes. The multiple wells at MSEEL 2 and the new generation high resolution fiber and LWD tools will provide 100's of terabytes of data in a series of similar wells under controlled conditions to test and enhance the understanding of shale reservoirs, MSEEL 2 will test new technologies and approaches to provide robust models that can be modified in near real-time using "thick" relatively high-cost data sets limited to science wells, or when calibrated more cost-effective "thin" data sets that could be used in broader field development and basin evaluation.

Figure 1.1: Boggess Pad with new generation permanent fiber in the central well (Boggess 5H, red star)) and deployable fiber in adjoining wells skipping one (orange stars). We will be able to monitor in near-real time fracture stimulation in the central 3 wells (3H, 5H and 9H). A vertical pilot will be drilled, cored and logged.

Project Management Update

Approach

The project management team will work to generate timely and accurate reporting, and to maintain project operations, including contracting, reporting, meeting organization, and general oversight.

Results and Discussion

The project team is tracking eight (8) milestones in this budget period.

	Task	Milestone	Status	Due Date
1.	2.1.2	Develop kerogen models of shale from different zones of MSEEL well and compare them to shales from wells in other parts of the basin	Complete Kerogen samples extracted from sidewall cores covering the whole Marcellus formation (ranging from Marcellus Top to Marcellus-Onondaga transition) have been analyzed using 13C NMR. New schematic kerogen models are being developed using lattice parameters and being compared to models of kerogen derived from wells in less mature part of the basin. Plan to synthesize results and submit publications in Fall 2018.	9/30/2018
2.	2.1.8	Geostatistical Well Analysis	Complete A paper was presented at URTeC (July) on a predictive data-driven machine learning model to understand the MSEEL well's performance and forecast the gas production using DTS data and daily flowing time as dynamic inputs. Papers using image analysis and nitrogen adsorption to quantify nano-pores in the Marcellus have been submitted.	9/30/2018
3.	2.1.7	Improved Reservoir Simulation for field implementation	Complete but will continue to be enhanced with continued production monitoring, and will be presented at URTeC this summer An improved history match that incorporates the unconventional fracture model and how to use this knowledge to increase production, efficiently space laterals and reduce cost. A manuscript has been accepted for presentation to the	10/31/2018

			Society of Petroleum Engineers Annual Meeting.	
4.	2.1.5	Create a Comprehensive Fracture Model	Complete but will continue to be enhanced with continued production monitoring, and will be presented at URTeC this summer A provisional patent application for analysis of fiber-optic data is moving forward. Papers are accepted for fall meetings of SPE, URTeC and AAPG.	11/30/2018
5.	2.2.1	Completion of four additional methane audits to further assess temporal variability in methane emissions	Complete Four previous audits have shown significant temporal variability. Four or more (up to 8 more over 2 years) audits well help us understand (by increasing sample size) if variability correlates with temporal production, cumulative production, age, water production, or seasonal variability. Initial results are presented in Jan 2019 report, publications are possible.	12/31/2018
6.	2.1.2	Understanding the type, amount and origin of natural gas	On Track Data analysis and interpretations of pyrolysis data are currently underway. We expect to generate some preliminary data and make some conference presentations in Fall 2018 and submit publications by Spring 2019	3/30/2019
7.	2.2.1	Successful deployment of an open path methane monitoring system during site audits	On Track Industry seeks to reduce costs of audits and streamline greenhouse gas reporting programs. This will teach us if near-field, indirect quantification or detection methods are applicable to the Appalachia region, versus the well-established research in relatively flat and calm Barnett and Fayetteville plays.	3/30/2019
8.	2.2.1	Characterize chemical transformations during produced water storage from well 3H	On Track Will complete characterization of changes in produced water chemistry (specifically Fe, Sr, Ba, Ra 226, Ra 228) and biological activity (CO_2 and CH_4 production) that occur during short term storage (20 days). Measures of Ra	3/30/2019

			activity (Ra 226 and Ra 228) of the solid precipitate formed during short term storage of produced water will also be completed.	

Topic 1 – Geologic Engineering

Approach

In addition to advances in improving our understanding of chemical evolution of produced water, methane emissions, microbiology and rock-fluid geochemistry, we completely revised the production simulation model integrating modeling results using all the subsurface and production data for both the MSEEL 3H and 5H wells. Especially important were the results made possible by development of a software system (FIBPRO) to analyze fiber-optic distributed acoustic sensing (DAS) and distributed temperature sensing (DTS) data and has been used to analyze the MSEEL data[1,2] Microseismic monitoring, fiber-optic distributed acoustic sensing (DAS), and distributed temperature sensing (DTS) observations made during the hydraulic fracture stimulation of the MIP-3H well were integrated with the production monitoring using the production log and ongoing DTS monitoring. The presence of long-period long-duration (LPLD) events, similar in appearance to tectonic tremors, were documented in the microseismic events generated during stimulation of the MIP-3H. LPLD events are generally overlooked but reveal the presence of significant deformation produced during hydraulic fracture stimulation. The distribution of this deformation and cross-flow between stages including LPLD events and DAS monitoring through the fiber-optic and microseismic data demonstrates the differences in completion efficiency among stages. This deformation effects and differences between stages and clusters affects production efficiency of the different stages, which is shown by the DTS over the last two years[3]. We now better understand the geologic/geomechanical controls on completion and ultimately on production at the stage level and can demonstrate a 10-15% increase in production for stages that are engineered.

Using a geomechanical model, a Discrete Natural Fracture (DFN) model was created and used to determine the complexity of hydraulic fracture geometry simulated through complex fracture models on the two new wells of the MSEEL pad (MIP-3H and MIP-5H)[4]. The microseismic and fiber-optic data obtained during the hydraulic fracture simulations served as constraining

[1] Ghahfarokhi, P. K., Carr, T., Song, L., Shukla, P., & Pankaj, P., 2018, Seismic Attributes Application for the Distributed Acoustic Sensing Data for the Marcellus Shale: New Insights to Cross-Stage Flow Communication. SPE Hydraulic Fracturing Technology Conference and Exhibition. Society of Petroleum Engineers, Paper 189888.
[2] Ghahfarokhi, P. K., Thomas Wilson, Abhash Kumar and Tim Carr, in press, Integrating Distributed Acoustic Sensing (DAS) and Borehole 3C Geophone Array Data to Identify Long-Period Long-Duration Seismic Events during Stimulation of a Marcellus Shale Gas Reservoir, Interpretation
[3] Carr, Timothy R., Payam Kavousi Ghahfarokhi, BJ Carney, Jay Hewitt and Robert Vagnetti, 2018, A New Algorithm for Processing Distributed Temperature Sensing (DTS), Conference Proceedings Eastern Section Society Petroleum Engineers, Society Petroleum Engineers, SPE-194814-18ERM-MS, 16p.
[4] Pankaj, Piyush, Shukla Priyayrat, Kavousi, Payam, Timothy Carr, 2018, Integrated Well Interference Modeling Reveals Optimized Well Completion and Spacing in the Marcellus Shale, Proceedings of Society Petroleum Engineers Annual Meeting and Technical Conference, SPE-191393, https://doi.org/10.2118/191393-MS, 16p.

parameters for the hydraulic fracture footprint on these wells. Sensitivity to the DFN is realized by parametric variations of DFN properties to achieve a calibrated fracture geometry. Reservoir simulation and history matching the well production data confirmed the subsurface production response to the hydraulic fractures.

Results and Discussion

Well spacing sensitivity was done to reveal the optimum distance that the wells need to be spaced to maximize recovery and number of wells per section. Naturally fractured reservoirs such as the Marcellus shale require an integrated reservoir modeling approach to determine well spacing and well-to-well interference. The geomechanical model was prepared with interpreted vertical log data. A discrete natural fracture (DFN) model was created and used to determine the complexity of hydraulic fracture geometry simulated through complex fracture models. The microseismic and fiber-optic data obtained during the hydraulic fracture simulations served as a constraining parameter for the hydraulic fracture footprint in the MSEEL wells. Sensitivity to the DFN was determined by parametric variations of DFN properties to achieve a calibrated fracture geometry. Reservoir simulation and history matching the well production data confirmed the subsurface production response to the hydraulic fractures. Well spacing sensitivity was revealed the optimum distance that the wells need to be spaced to maximize recovery and number of wells per section.

Hydraulic fracture geometry was found to be a result of the calibration parameters, such as horizontal stress anisotropy, fracturing fluid leak-off, and the DFN. The availability of microseismic data and production history matching through integrated numerical simulation are critical elements to bring unique representation of the subsurface reaction to the injected fracturing fluid. The approach developed can be consistently applied to evaluate well spacing and interference in time for the subsequent wells completed in the Marcellus. With the current completion design and pumping treatments, the optimal well spacing of 990 ft was determined between the wells. However, wells to be completed in the future this needs to be tested due to the heterogeneity in the reservoir properties to ensure that wells are not either underspaced to cause well production interference or overspaced to create upswept hydrocarbon reserves in the formation.

Products

We now have results that can improve the modeling of activation and movement on individual fracture swarms and will work to history match at the individual stage and sum to the well. This will be a challenge, but the DAS, DTS and log data do provide the basis.

Plan for Next Quarter

Work to understand the effects of individual fractures on completion efficiency. Will individual fractures respond to stimulation using geomechanical properties and simple geomechanical approaches?

Topic 2 – Geophysical & Geomechanical

Approach

Geophysical and Geomechanical

During this quarterly period, the influence of a discrete fracture network on the growth of hydraulic fractures was investigated through the use of numerical modeling. The numerical model updated in a previous quarter was used to compute hydraulic fracture dimensions for stage 26 through stage 30 of well MIP-5H.

Results & Discussion

Geophysical

Microseismic monitoring by downhole geophones, surface seismic, fiber-optic distributed acoustic sensing (DAS), and distributed temperature sensing (DTS) observations were made during the hydraulic fracture stimulation of the MIP-3H well in the Marcellus Shale in northern West Virginia. DAS and DTS data measure fiber strain and temperature, respectively, along a fiber optic cable cemented behind the casing of the well. The presence of long-period long-duration (LPLD) events were evaluated in the borehole geophones, DAS data, and surface seismic data of one of the MIP-3H stimulated stages. LPLD events are generally overlooked during the conventional processing of microseismic data, but they represent significant non-brittle deformation produced during hydraulic fracture stimulation. In a single stage that was examined 160 pre-existing fractures and two faults of suboptimal orientation are noted in the image logs. We identified two low-frequency (<10HZ) events of large temporal duration (tens of seconds) by comparing the surface seismic data, borehole geophone data, and DAS amplitude spectra of one of the MIP-3H stages. Spectrograms of DAS traces in time and depth reveals that the first low frequency event might be an injection noise that has footprints on all DAS channels above the stimulated stage. However, the surface seismic array shows a LPLD event concurrent with the first low frequency event on DAS. The second LPLD event on DAS data and surface seismic data is related to a local deformation and does not have footprints on all DAS channels. The interpreted LPLD events are less than 100s long, are in frequencies less than 10Hz, and are accompanied with microseismic activity. Read More: https://library.seg.org/doi/10.1190/int-2018-0078.1

Geomechanical

Table 2.1 shows the computed hydraulic fracture geometries for numerically modeled MIP-5H stage 26 through stage 30. Figure 2.1 shows the hydraulic fracture geometry for one of the primary induced hydraulic fractures in stage 30 of well MIP-5H. Figure 2.2 shows the cumulative proppant mass versus time (calculated and measured), Figure 2.3 shows the cumulative slurry volume injected versus time (calculated and measured), and Figure 2.4 shows the surface pressure versus time (calculated and measured) for stage 30 of well MIP-5H.

Microseismic data was available for all stages numerically modeled during this quarterly period for well MIP-5H. Microseismic, well, and hydraulic fracture geometry data were visualized in three dimensions. Figure 2.5 through Figure 2.9 show side views of numerically modeled hydraulic fracture geometries and available measured microseismic events and magnitudes for stage 26 through stage 30, respectively, for well MIP-5H. Figure 2.10 shows an overview of the hydraulic fractures numerically modeled this quarter, as well as available microseismic event

data and the entire MIP-5H wellbore. Figure 2.11 shows a top view of all numerically modeled hydraulic fracture geometries this quarter with available microseismic event data and the nearby section of the MIP-5H wellbore. Figure 2.12 shows an orthogonal projection of the numerically modeled hydraulic fracture geometries this quarter with available microseismic event data and the nearby section of the MIP-5H wellbore.

Vertical hydraulic fracture growth information was available from Schlumberger and was compared with numerical model predictions. Figure 2.13 through Figure 2.19 show side views of calculated primary hydraulic fractures, measured microseismic events and magnitudes, and Schlumberger vertical fracture growth estimates for stage 9 through stage 15 of well MIP-5H. The upper red line indicates Schlumberger's interpretation of the extent of upward hydraulic fracture growth, while the lower red line indicates Schlumberger's interpretation of the extent of downward hydraulic fracture growth based on microseismic data analysis.

Table 2.1: Computed Hydraulic Fracture Geometries – Stage 26 through Stage 30 – MIP-5H

STAGE	Fracture Half-Length (ft)	Fracture Height (ft)	Average Fracture Width (in)
26	618.4	323.7	0.027296
27	617.7	316.5	0.025959
28	599.4	318.5	0.025006
29	644.6	329.5	0.030494
30	644.1	336.8	0.03046

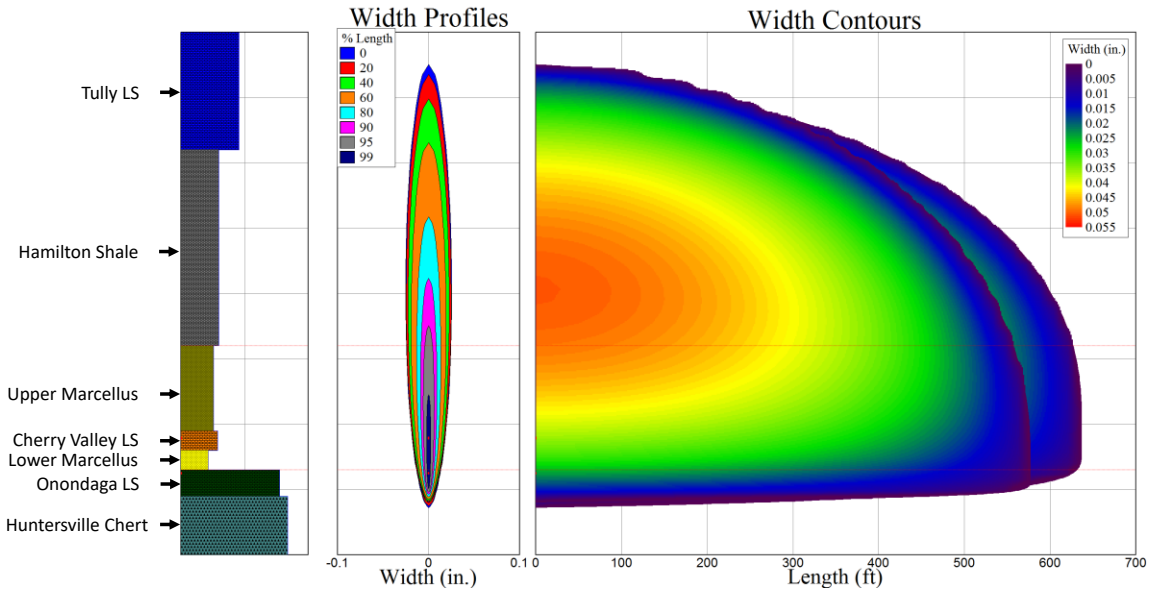

Figure 2.1: Primary Hydraulic Fracture Geometry for Stage 30 – MIP-5H

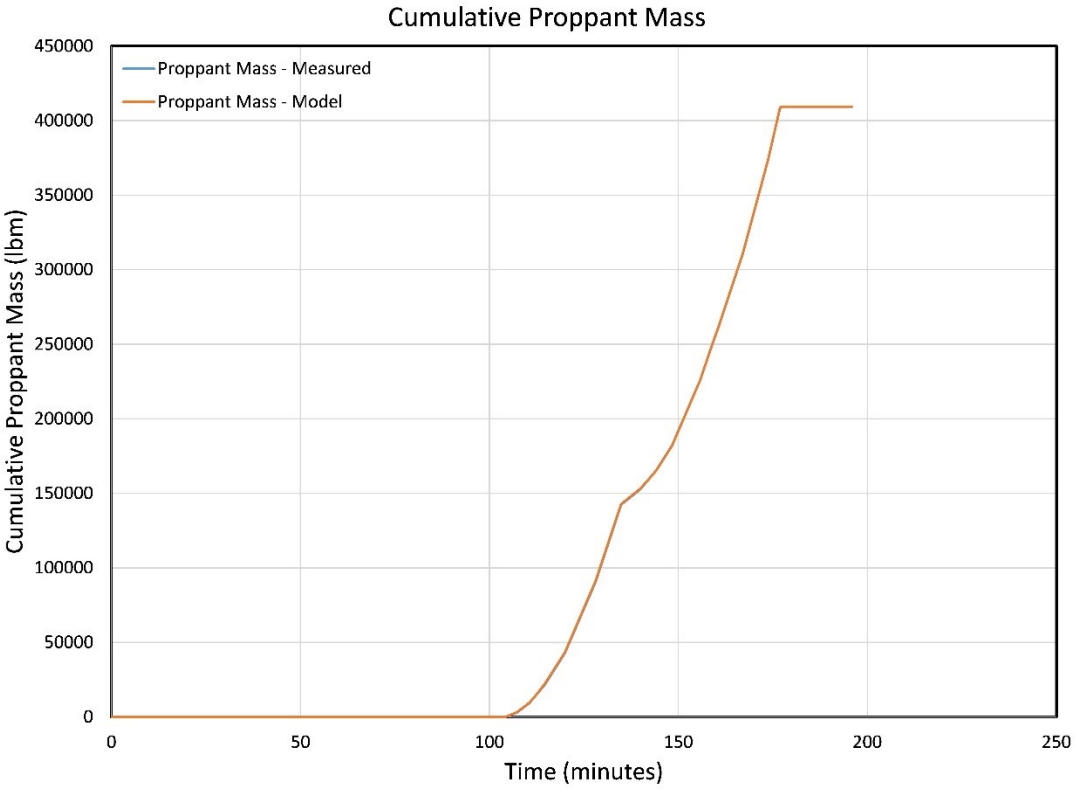

Figure 2.2: Cumulative Proppant Mass Injected for Stage 30 – MIP-5H

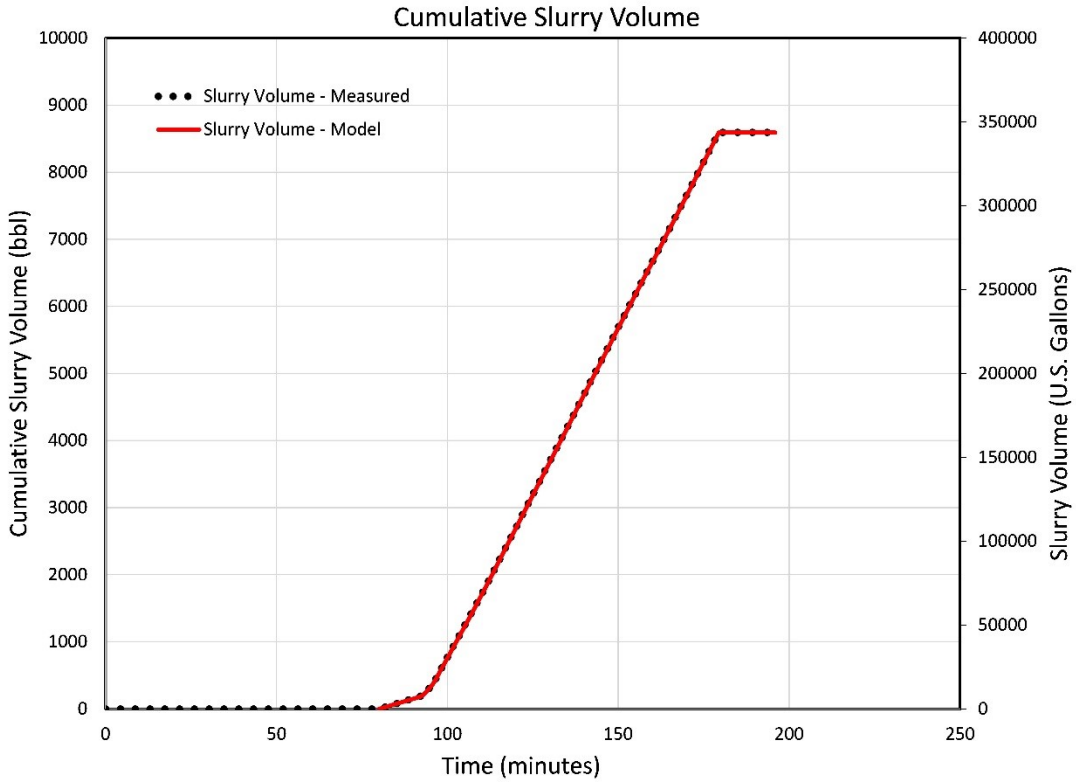

Figure 2.3: Cumulative Slurry Volume Injected for Stage 30 – MIP-5H

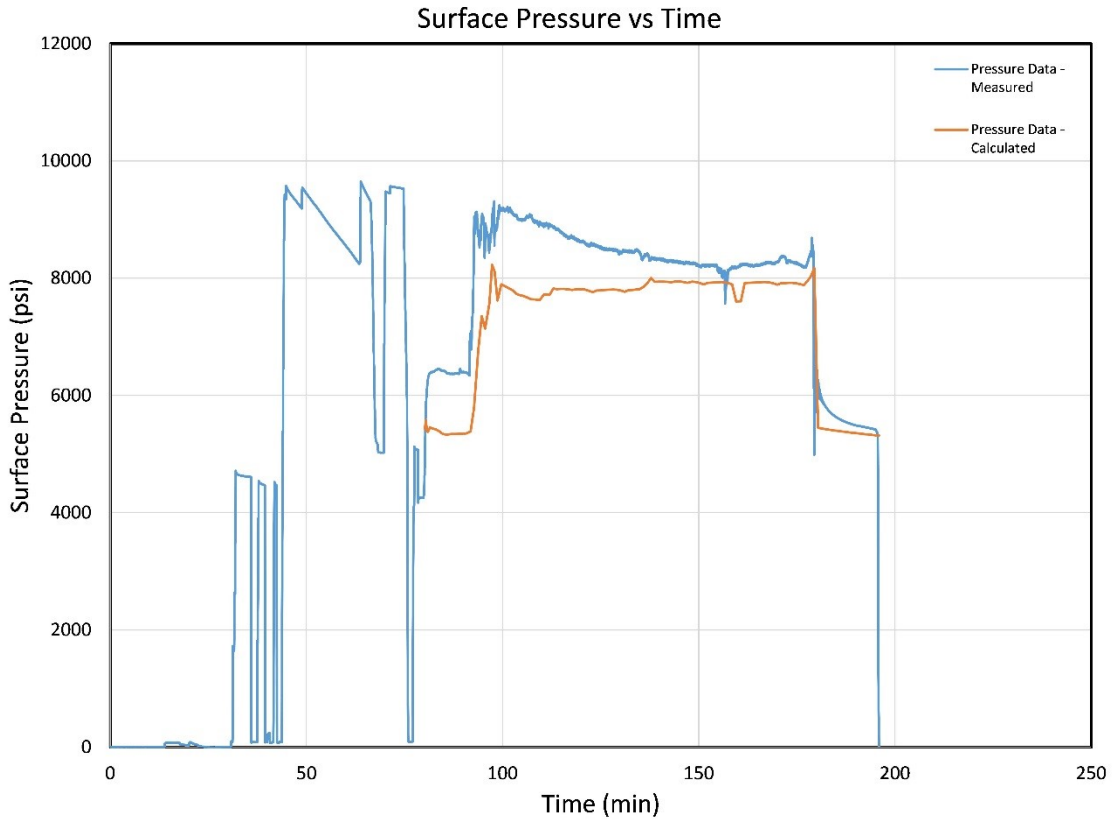

Figure 2.4: Surface Pressure versus Time for Stage 30 – MIP-5H

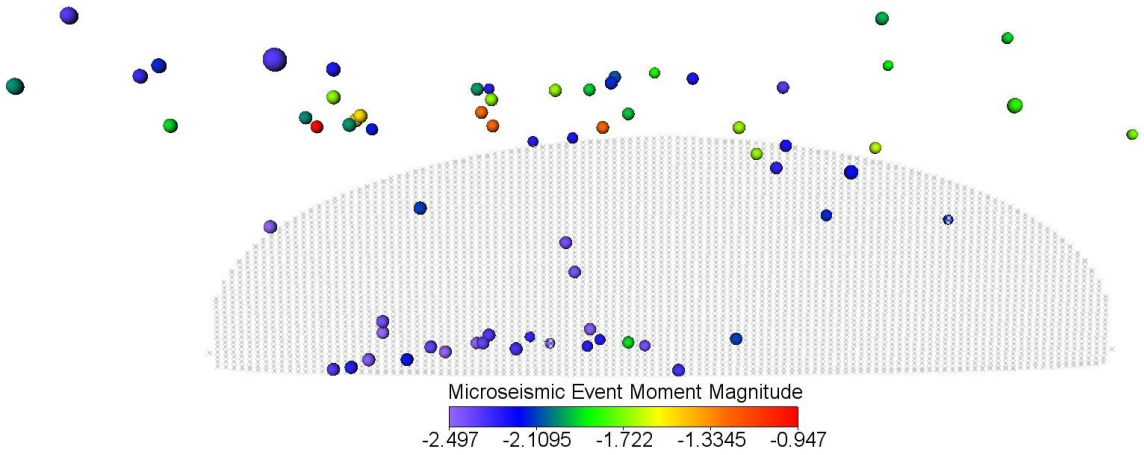

Figure 2.5: Side View of Calculated Primary Hydraulic Fracture and Measured Microseismic Events and Magnitudes for Stage 26 – MIP-5H

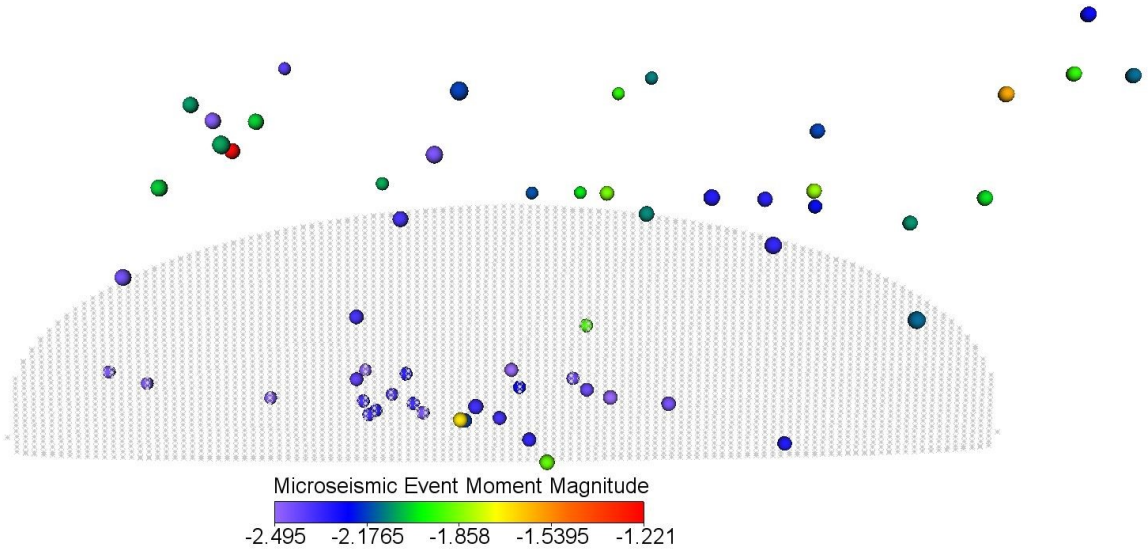

Figure 2.6: Side View of Calculated Primary Hydraulic Fracture and Measured Microseismic Events and Magnitudes for Stage 27 – MIP-5H

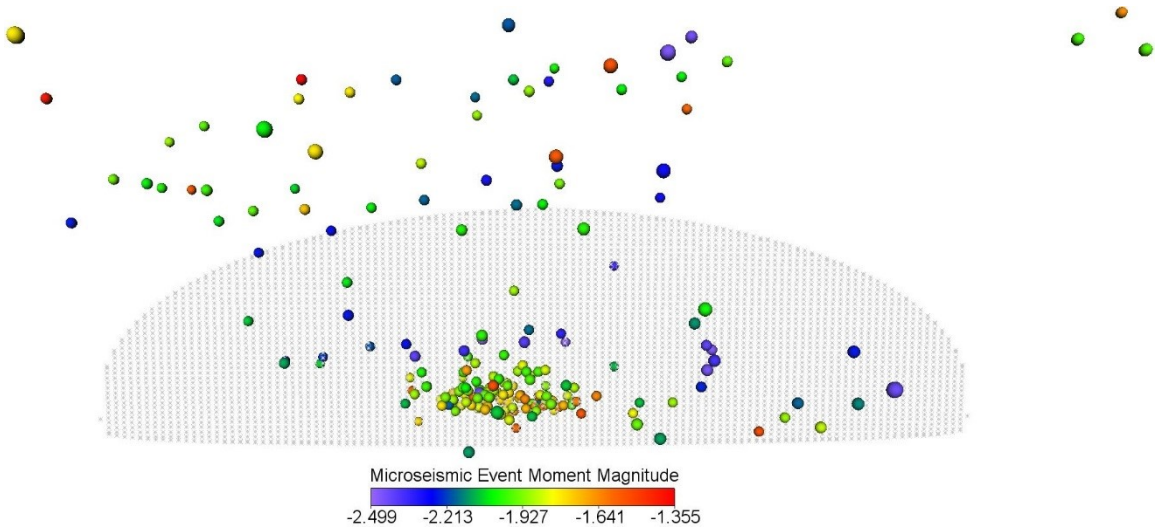

Figure 2.7: Side View of Calculated Primary Hydraulic Fracture and Measured Microseismic Events and Magnitudes for Stage 28 – MIP-5H

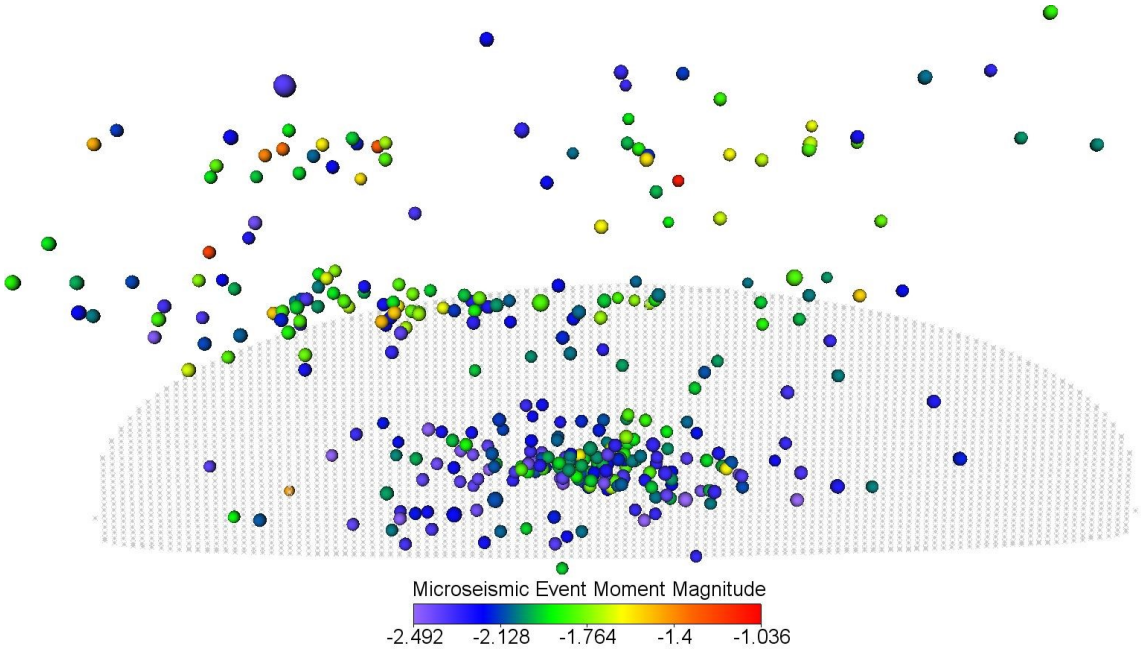

Figure 2.8: Side View of Calculated Primary Hydraulic Fracture and Measured Microseismic Events and Magnitudes for Stage 29 – MIP-5H

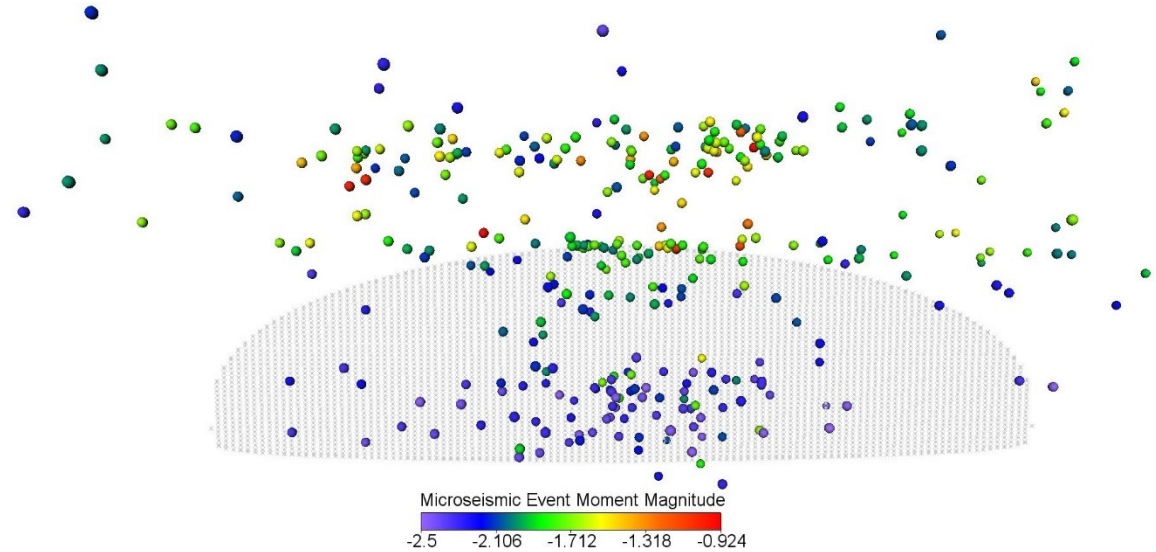

Figure 2.9: Side View of Calculated Primary Hydraulic Fracture and Measured Microseismic Events and Magnitudes for Stage 30 – MIP-5H

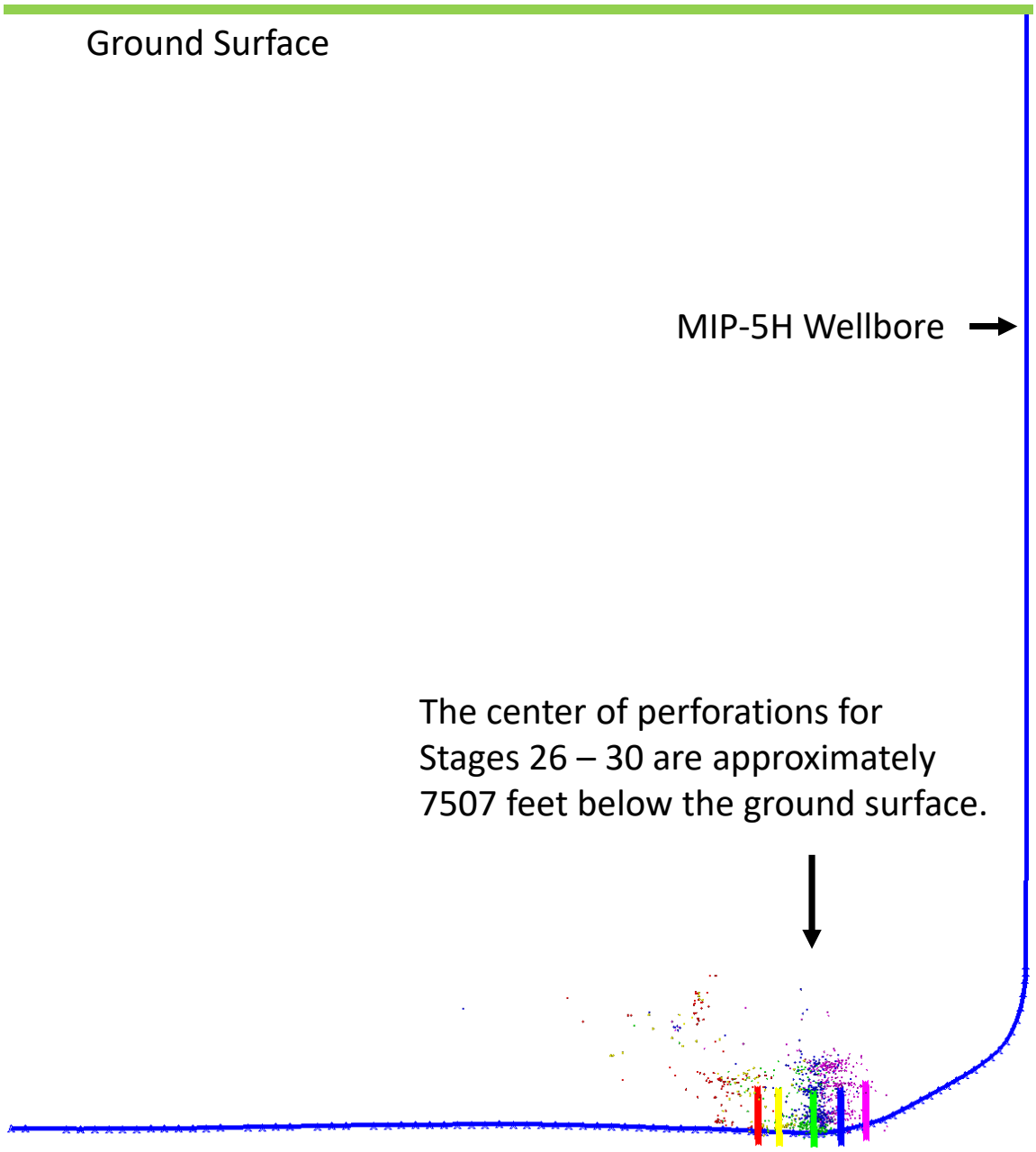

Figure 2.10: Overview of Calculated Primary Hydraulic Fracture Geometries, Available Measured Microseismic Events, and Entire Wellbore for Stage 26 through Stage 30 – MIP-5H

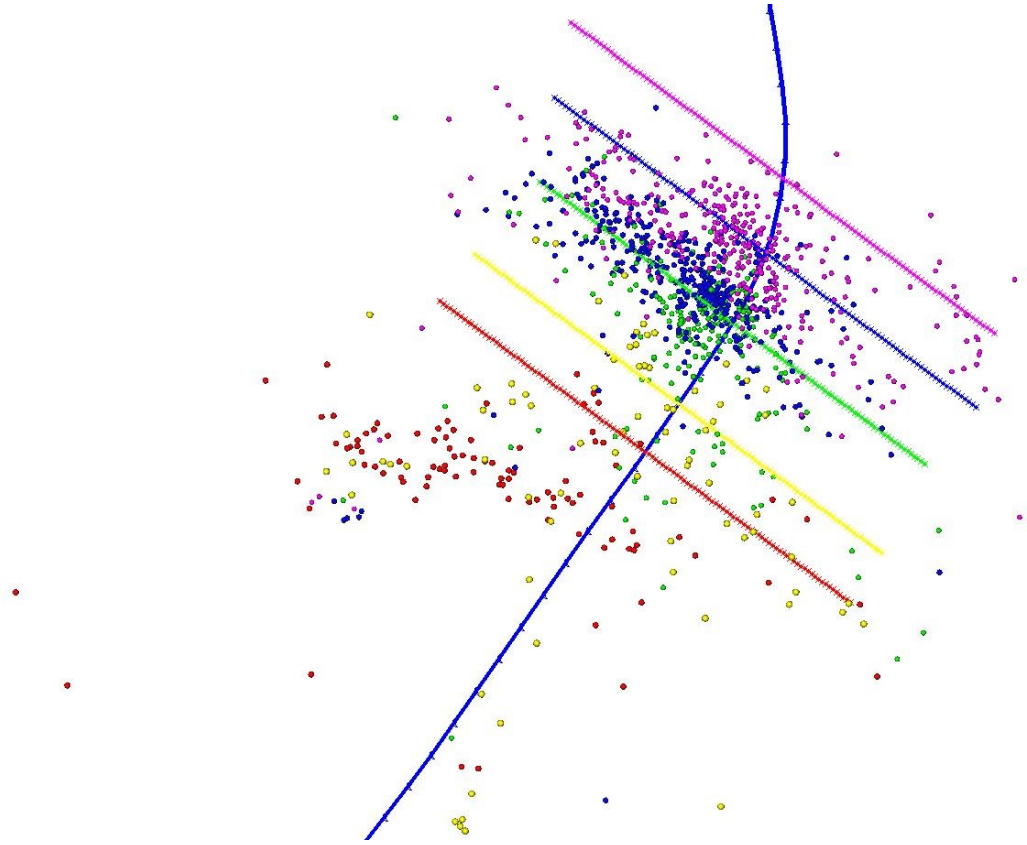

Figure 2.11: Top View of Calculated Primary Hydraulic Fracture Geometries, Available Measured Microseismic Events, and Nearby Wellbore for Stage 26 through Stage 30 – MIP-5H

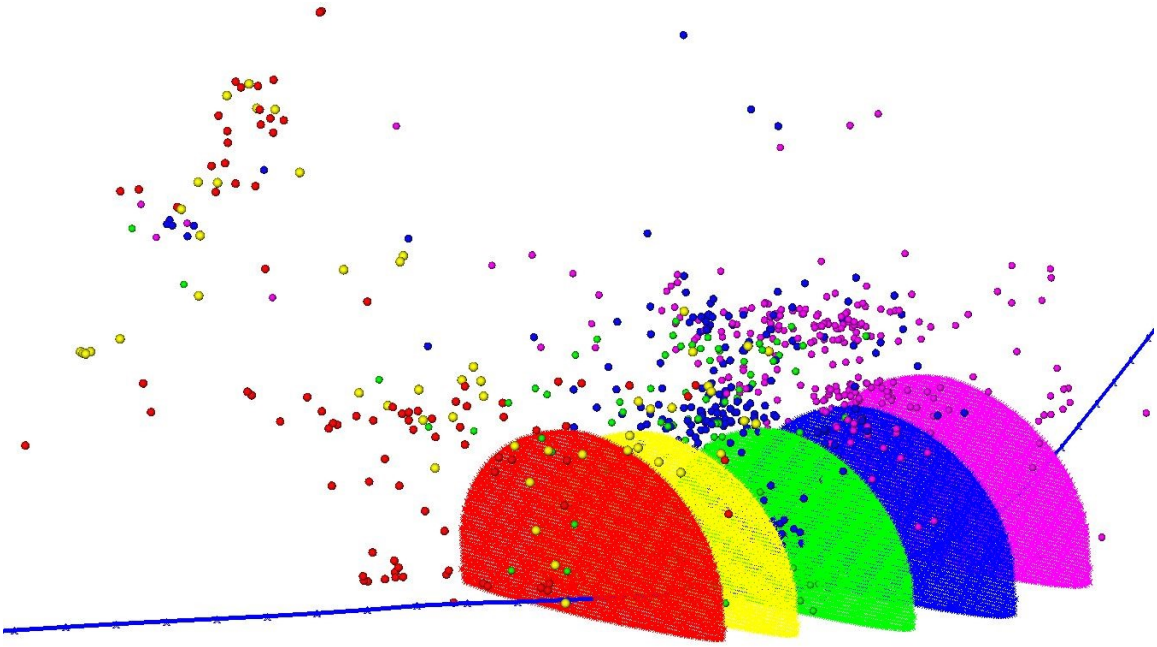

Figure 2.12: Orthogonal View of Calculated Primary Hydraulic Fracture Geometries, Available Measured Microseismic Events, and Nearby Wellbore for Stage 26 through Stage 30 – MIP-5H

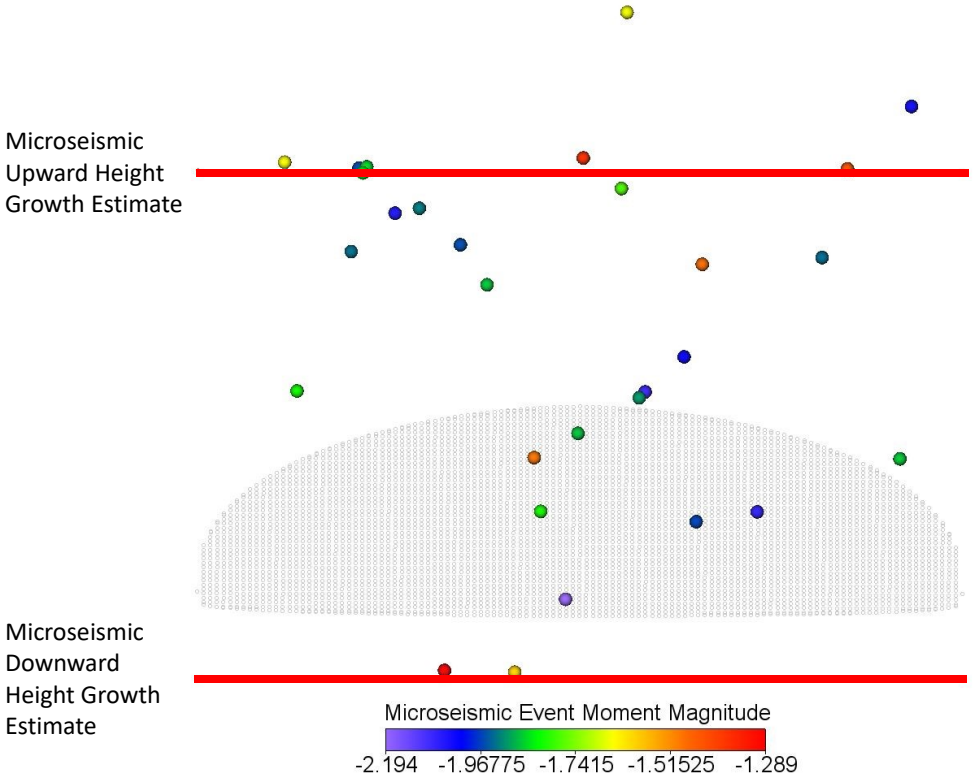

Figure 2.13: Side View of Calculated Primary Hydraulic Fracture, Measured Microseismic Events and Magnitudes, and Schlumberger Microseismic Height Growth Estimates for Stage 9 – MIP-5H

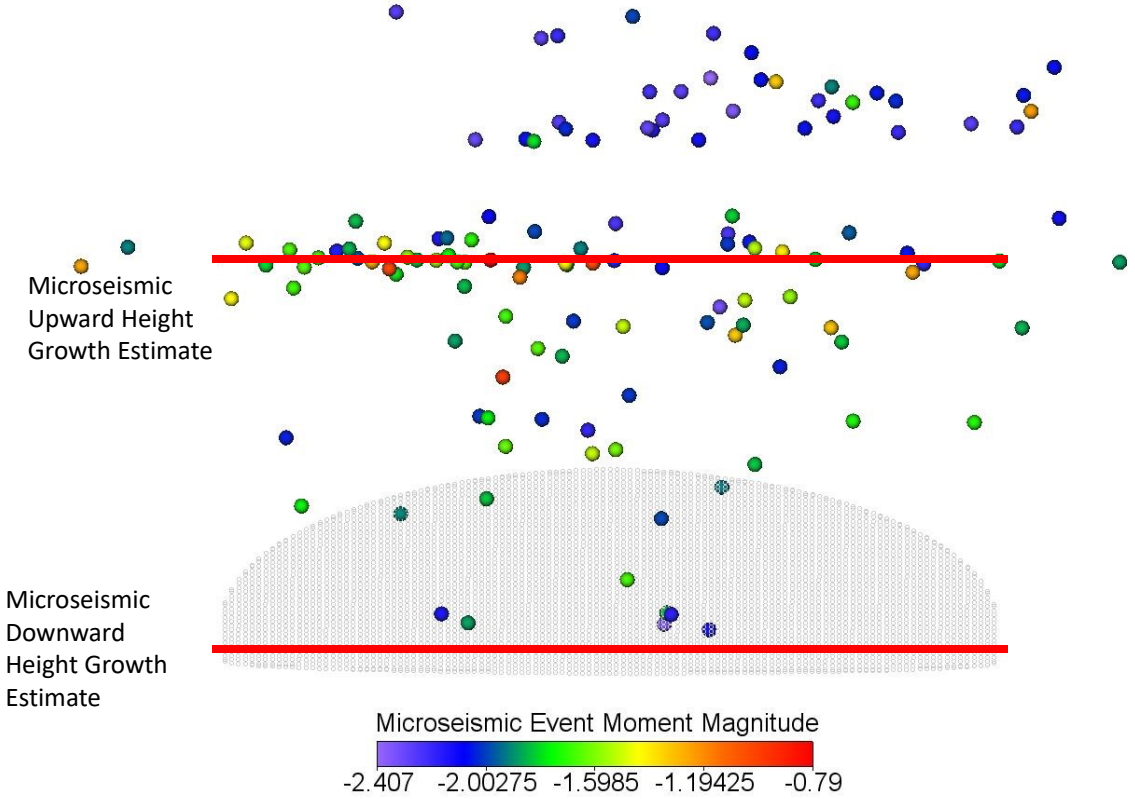

Figure 2.14: Side View of Calculated Primary Hydraulic Fracture, Measured Microseismic Events and Magnitudes, and Schlumberger Microseismic Height Growth Estimates for Stage 10 – MIP-5H

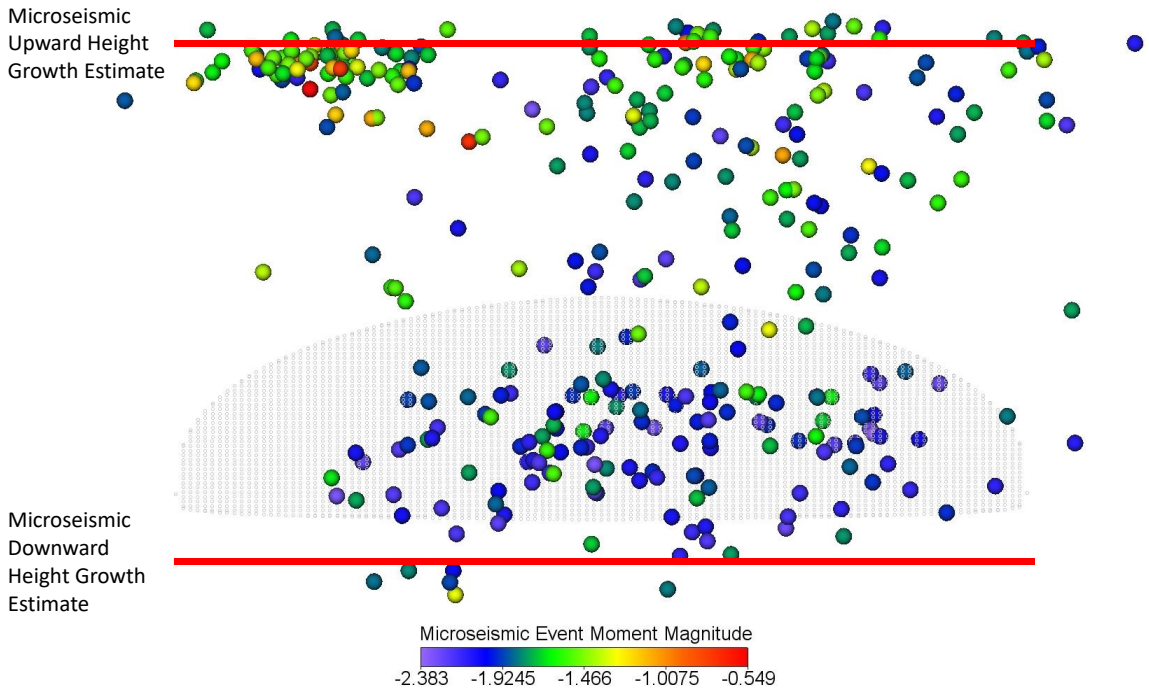

Figure 2.15: Side View of Calculated Primary Hydraulic Fracture, Measured Microseismic Events and Magnitudes, and Schlumberger Microseismic Height Growth Estimates for Stage 11 – MIP-5H

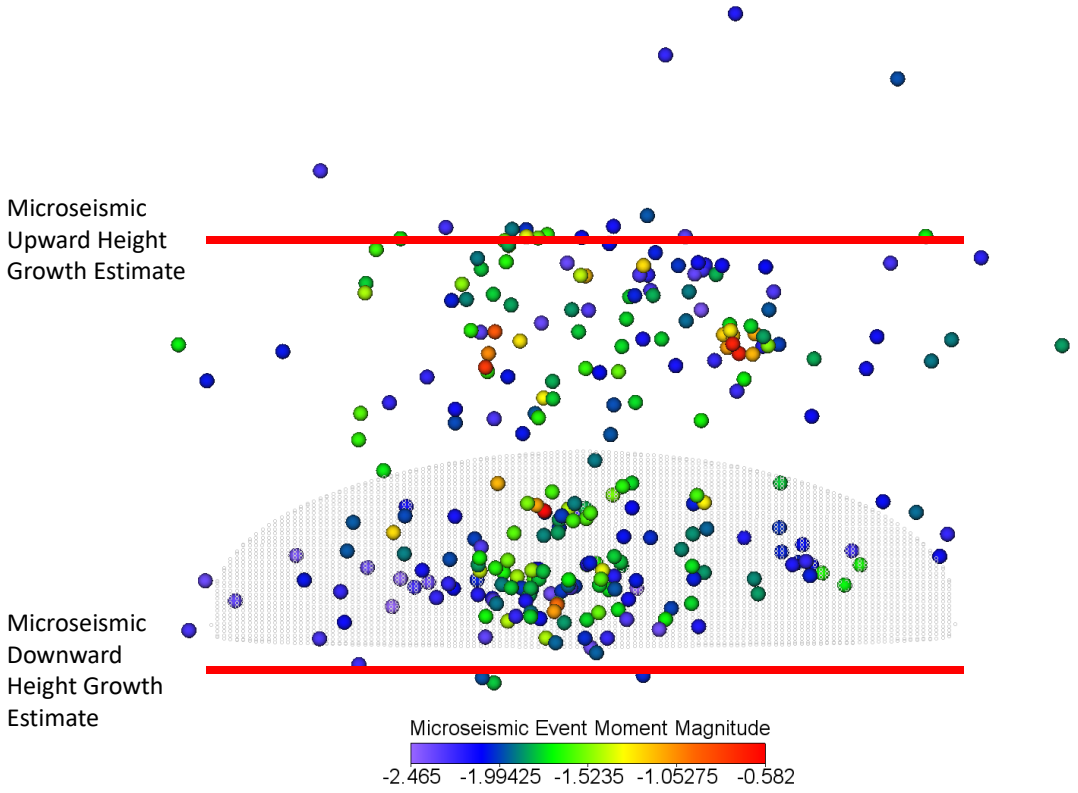

Figure 2.16: Side View of Calculated Primary Hydraulic Fracture, Measured Microseismic Events and Magnitudes, and Schlumberger Microseismic Height Growth Estimates for Stage 12 – MIP-5H

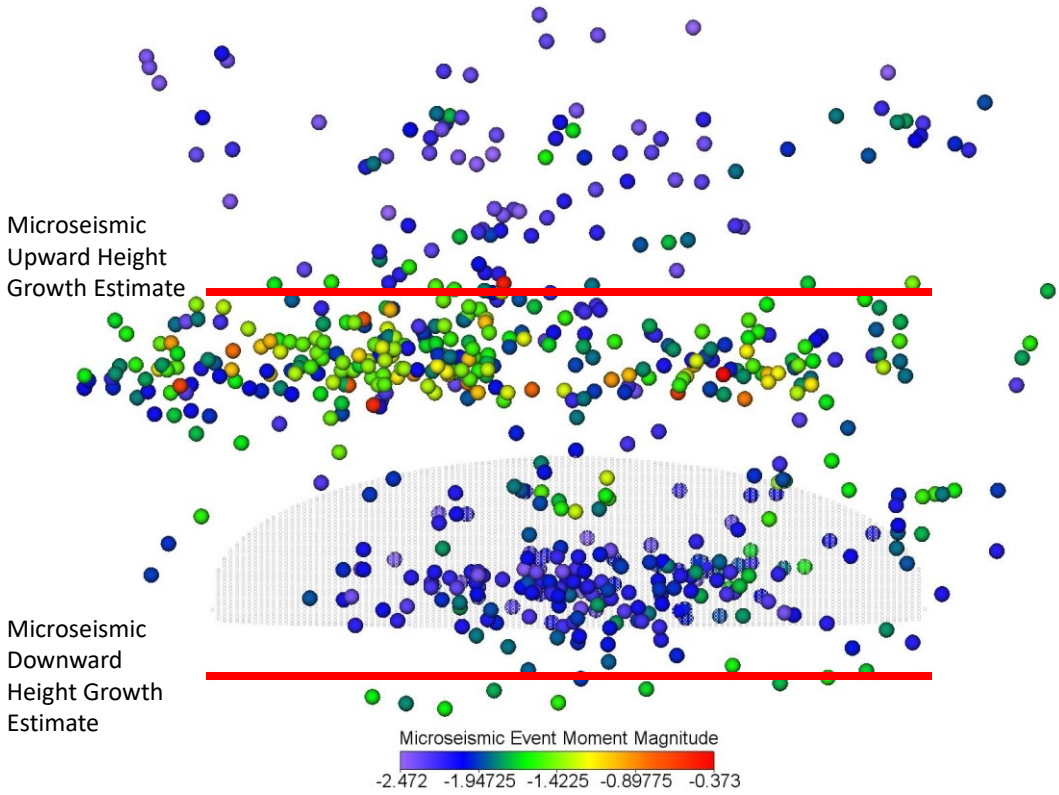

Figure 2.17: Side View of Calculated Primary Hydraulic Fracture, Measured Microseismic Events and Magnitudes, and Schlumberger Microseismic Height Growth Estimates for Stage 13 – MIP-5H

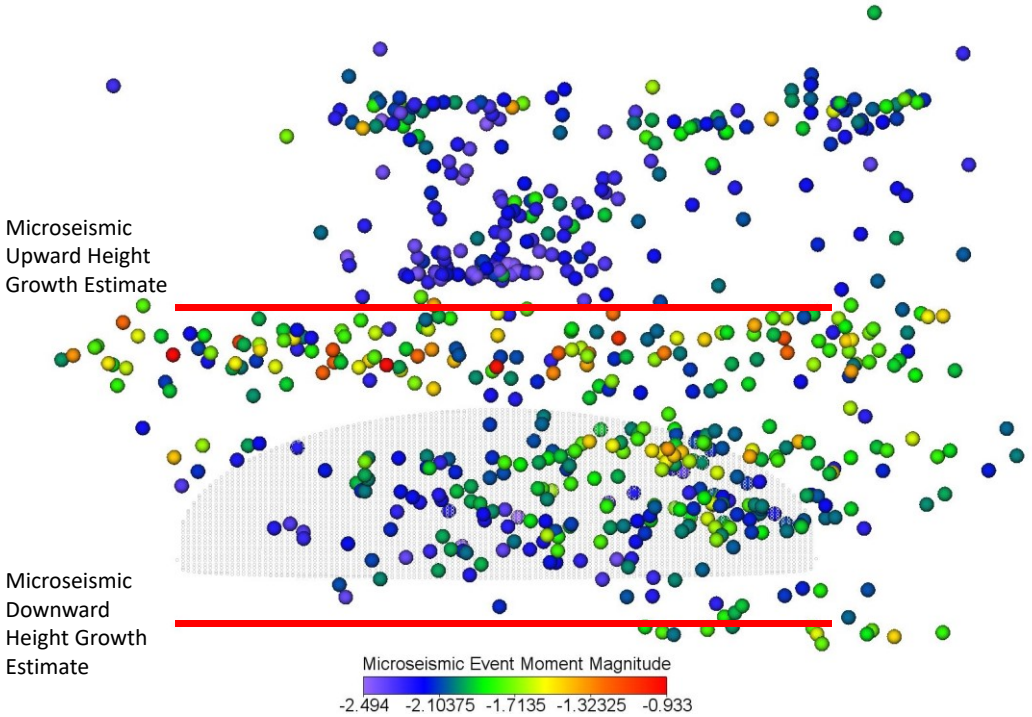

Figure 2.18: Side View of Calculated Primary Hydraulic Fracture, Measured Microseismic Events and Magnitudes, and Schlumberger Microseismic Height Growth Estimates for Stage 14 – MIP-5H

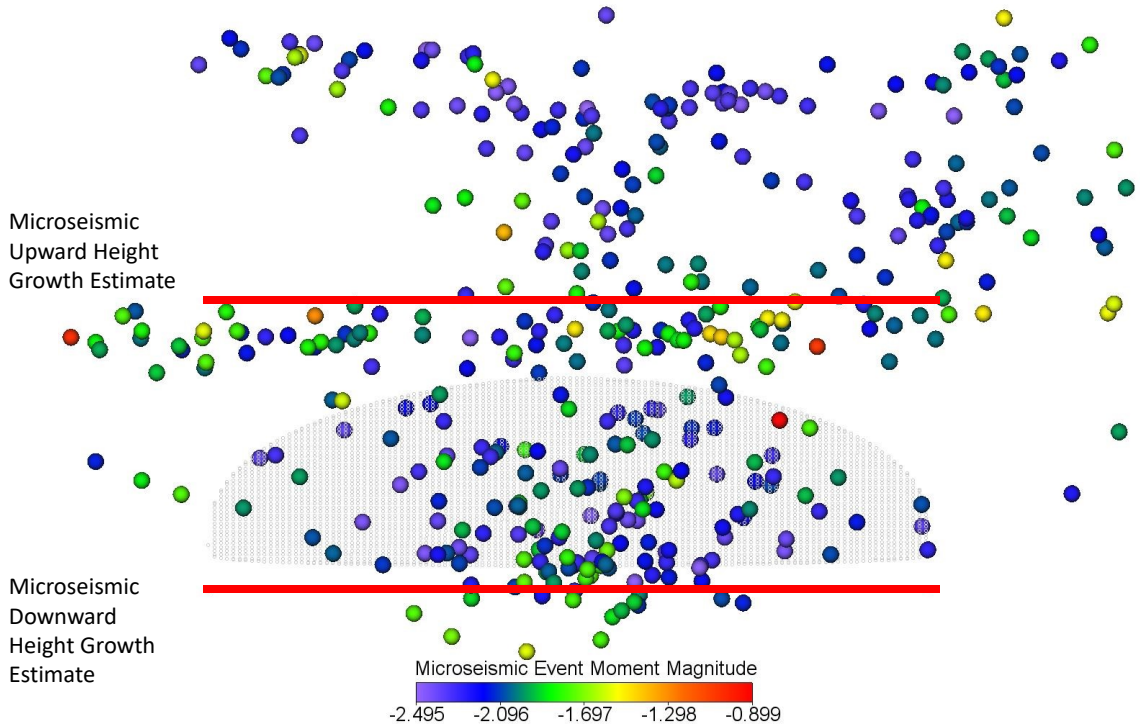

Figure 2.19: Side View of Calculated Primary Hydraulic Fracture, Measured Microseismic Events and Magnitudes, and Schlumberger Microseismic Height Growth Estimates for Stage 15 – MIP-5H

Products

N/A

Plan for Next Quarter

Geophysical and Geomechanical

The modeling study will be continued to investigate the reported microseismic height estimates by Schlumberger versus the numerical model predictions of hydraulic fracture heights. If needed, additional hydraulic fracture modeling work will be completed through the use of available information on the hydraulic fracturing field parameters (fluid volumes, pumping rate, proppant schedule, and geophysical data).

Additionally, the influence of fluid and geomechanical properties on surface treatment pressures will be investigated. Fluid and geomechanical properties will be modified in order to explore the possibility of a better match with reported surface pressures and microseismic-based fracture heights reported by Schlumberger.

Topic 3 – Deep Subsurface Rock, Fluids, & Gas

Approach

The approach is to work across a broad spectrum of detailed geochemical and biogeochemical investigations that could have significant impact on completion and production.

Results & Discussion

Sharma's Lab

1. **Understanding spatial heterogeneity of kerogen across the entire Marcellus basin** Vikas Agrawal determined the heterogeneities present in kerogen structure within a particular kerogen "type" across the entire Marcellus basin by constructing kerogen unit structures.. Our observations indicate that the molecular structure of kerogen within a particular kerogen "type" and maturity can be very different and a unique kerogen structural model does not exist. The heterogeneities observed in different samples of a particular kerogen "type" can be due to variations in sources of (variable amount of biomolecules), paleo-redox conditions, microbial diagenesis, differential kerogen cracking mechanism, etc. The major conclusion of the study was that simulations of physicochemical properties of kerogen should be based on molecular parameters of kerogen extracted from specific part of the basin rather than using a general structural model based on kerogen "type."

   Deliverables: 1) Manuscript currently under review in the journal *Scientific Reports* 2) Present results in upcoming AAPG conference at San Antonio, Texas.

2. **Developing new regression models for kerogen extracted including MSEEL well.** Vikas Agrawal has published a manuscript in the journal *Scientific Reports* on accurately determining thermal maturity and hydrocarbon potential in Shale using kerogen structural parameters. The major finding of new models proposed in this study is that they were generated using kerogen extracted from samples across the entire maturity range of hydrocarbon generation including MSEEL well, and therefore more accurately represent the source rock in mature shale plays like Marcellus as compared to older models. It was observed that the correlation coefficient of immobile alkyl chains was highest followed by alkyl chains, then by total aromatic carbon and by total alkyl (without heteroatoms) as shown in Fig. 1. It was also determined that mobile and quaternary alkyl group, mobile

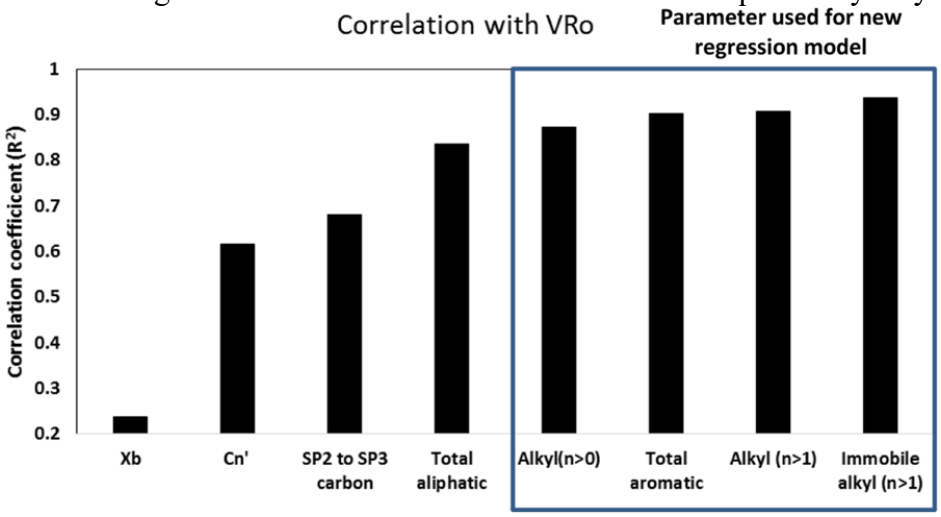

Figure. 3.1 Correlation of different structural parameters of kerogen with thermal maturity coefficient VRo.

methyl group and immobile alkyl chains had the highest correlation coefficient with hydrocarbon potential (Fig. 2). A new equation for determining the hydrocarbon potential that is based the fractions of these structural parameters was proposed.

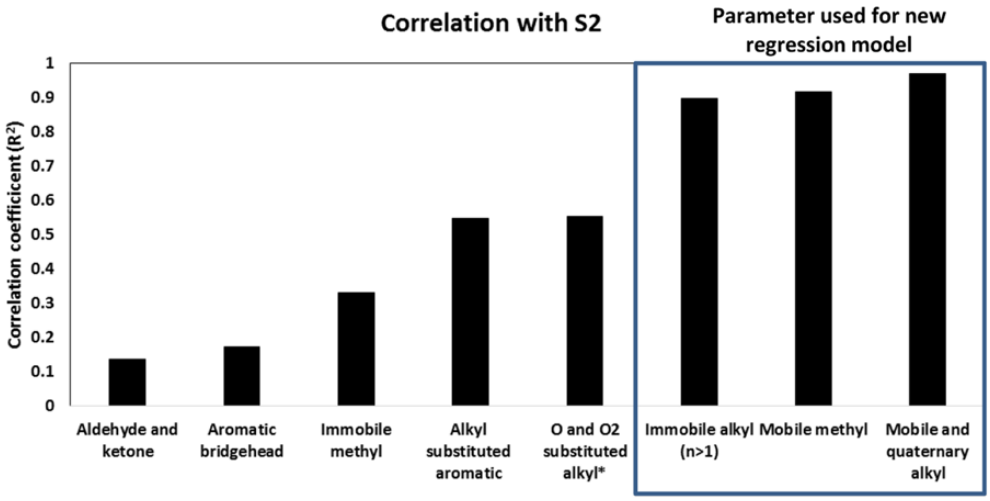

Figure. 3.2 Correlation of different structural parameters of kerogen with true HC potential (S2).

Deliverable: 1) A manuscript summarizing key finding is currently published in the journal *Scientific Reports*. 2) The results will be presented at in AAPG 2019, San Antonio, Texas.

3. **Experiments to understand kerogen-frac fluid and interaction:**

We re-submitted the manuscript on understanding the effect of maturity and mineralogy on shale fracturing fluid interactions, addressing all the major and minor revisions suggested by the journal reviewers. We are in the final step of extracting kerogen from all the shale samples used in these high P-T experiments to understand the effect on frac fluid interaction on kerogen molecular structure.

Deliverables: 1) A manuscript summarizing key finding is in acceptance stage in journal *Environmental Science: Processes & Impacts.* 2) Presented the results in GSA conference in Indianapolis, Indiana, 2018 3) Finish analysis of all kerogen samples using ^{13}C solid state NMR by summer 2019

4. **Understanding the type, amount and origin of gas.** Results from the open and closed pyrolysis experiments have been analyzed and quantified by V. Agrawal. We are in process preparing a manuscript to be submitted in the journal *Fuel*. The aliphatic and aromatic carbon chains present in the labile fraction of kerogen, determined by open system pyrolysis (Py-GC-FID) of the kerogen sample from lower Marcellus formation of the MSEEL well is shown in figure. 3 The chromatograms generated from the analysis shows the presence of n-alkanes and n-alkenes carbon chains ranging from n-1 to n-12. It also

shows the presence of aromatic chains: benzene, toluene, phenol. styrol, xylene, 1,2,4 tetramethyl benzene, naphthalene and 2- methyl naphthalene.

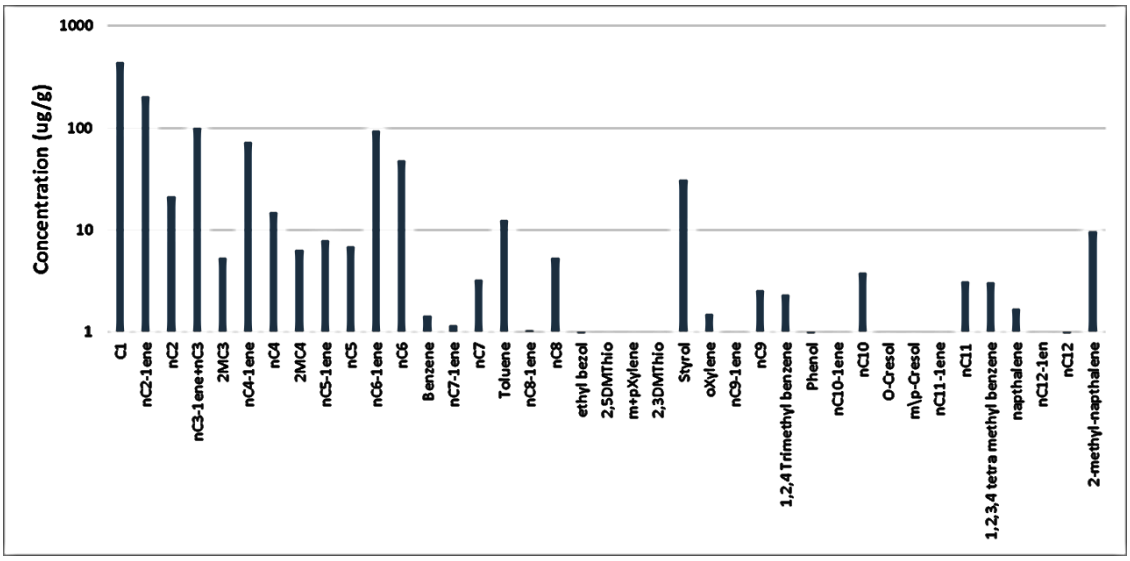

Figure 3.3 Aliphatic and aromatic carbon chains present in the labile fraction of kerogen at lower Marcellus formation at the MSEEL site.

Deliverable: Submit a manuscript to the journal Fuel by Spring- Summer 2019.

5. **Microbial lipid analysis of sidewall cores from MSEEL:** Ph.D. student Rawlings Akondi has published a manuscript in *Environmental Science: Processes and Impacts*. The manuscript examines the distribution of membrane lipid biomarkers (PLFA and DGFA) prior to energy development within and above the Marcellus Shale Formation into the overlying Mahantango Formation of the Appalachian Basin. The manuscript also highlights the importance of understanding the microbial community structure in black shales especially because of increase interest in hydrocarbon development in black shales. The paper differentiates the microbial signatures in the shale rock samples from the drilling muds, and provides potential evidence of indigenous membrane lipid profiles which could be indicative of native deep subsurface microbial life. We utilized the PLFA and DGFA signatures to (i) to evaluate trends in biomarker yield and variety across three geologic horizons, and (ii) to identify signature lipid biomarkers (SLB) and potential microbial groups within the subsurface rock cores. We reported higher variety and concentration of PLFA in the transition zone between the extremely low permeability Marcellus Shale Formation and the more permeable Mahantango Formation. Meanwhile the distribution and diversity of DGFA membrane profiles were higher in the Mahantango Formation. There were more stress indicative biomarkers such as the trans-membrane fatty acids, oxiranes, keto-, and dimethyl lipid fatty acids in the cores samples, a potential indication that the bacterial communities had experienced physiological stress or nutrient deprivation during or after deposition (Figure 4).

Figure 3.4. Venn diagram illustrating the distribution of the individual lipid fatty acids and functional group lipids for the PLFA (A and C) and DGFA (B and D) within the core samples, core washes, and drilling mud samples. Yellow represent lipid fatty acids detected only in the cores samples, the red represent profiles detected in the drilling mud samples only.

Deliverable: A manuscript reporting the results has been published in the Environmental Science: Processes & Impacts.

Effects of Sampling and Long Term Storage on Microbial Lipid Biomarker Distribution in Deep Subsurface Marcellus Shale Cores. Ph.D. student Rawlings Akondi has analyzed the lipid biomarkers to compare the distribution and yield between the recently collected MSEEL core samples and old surface stored WV 6 core samples. The paper uses the ester-linked phospholipid (PLFA) and diglyceride fatty acid (DGFA) analyses to examine the effects of sampling and storage conditions on the microbial community structure and composition of deep subsurface black shale cores.

Deliverables: The manuscript reporting the results will be submitted in *Frontiers in Microbiology* in this Spring 2019 Semester.

Wrighton's Lab (OSU-CSU); Wilkins Lab (OSU-CSU)

Milestone 1. This effort will compare the methane-generating *Methanohalophilus* strains across shales, many isolated from the MSEEL project. Genomics will be used to identify what makes persisting strains "unique" physiologically and then demonstrating this in the laboratory.

About 60% of natural gas production in the United States comes from hydraulic fracturing of unconventional reservoirs, such as shales or organic-rich micrites. This process inoculates and enriches for halotolerant microorganisms in these reservoirs over time, resulting in a saline ecosystem that includes methane producing archaea. Here, researchers survey the biogeography of methanogens across unconventional reservoirs, and report that members of genus Methanohalophilus are recovered from every hydraulically fractured unconventional reservoir sampled by metagenomics. The first genomic sequencing of three isolate genomes are provided, as well as two metagenome assembled genomes (MAGs). Utilizing six other previously sequenced isolate genomes and MAGs, researchers perform comparative analysis of the 11 genomes representing this genus. This genomic investigation revealed distinctions between surface and subsurface derived genomes that are consistent with constraints encountered in each environment. Genotypic differences were also uncovered between isolate genomes recovered from the same well, suggesting niche partitioning among closely related strains. These genomic substrate

utilization predictions were then confirmed by physiological investigation. Fine-scale microdiversity was observed in CRISPR-Cas systems of Methanohalophilus, with genomes from geographically distinct unconventional reservoirs sharing spacers targeting the same viral population. These findings have implications for augmentation strategies resulting in enhanced biogenic methane production in hydraulically fractured unconventional reservoirs.

Deliverable 1. The corresponding paper was recently published in *Environmental Microbiology*. Citation provided below:

Borton MA, Daly RA, O'Banion B, Hoyt DW, Marcus DN, Welch S, Hastings SS, Meulia T, Wolfe RA, Booker AE, Sharma S, Cole DR, Wunch K, Moore JD, Darrah TH, Wilkins MJ, and Wrighton KC (2018) Comparative genomics and physiology of the genus Methanohalophilus, a prevalent methanogen in hydraulically fractured shale. *Environmental Microbiology*. doi: 10.1111/1462-2920.14467

Milestone 2. Completion of laboratory investigations studying Halanaerobium growth under pressure conditions characteristic of deep shale ecosystems.

Bacterial *Halanaerobium* strains become the dominant persisting microbial community member in produced fluids across geographically distinct hydraulically fractured shales. *Halanaerobium* is not native to the shale formations, but is inadvertently introduced during the drilling and fracturing process and must therefore tolerate large changes in pressure, temperature, and salinity. Here, researchers used a *Halanaerobium* strain isolated from a natural gas well in the Utica Point Pleasant formation to investigate metabolic and physiological responses to growth under high-pressure subsurface conditions. Laboratory incubations confirmed the ability of *H. congolense* strain WG8 to grow under pressures representative of deep shale formations (21-48 MPa). Under these conditions, broad metabolic and physiological shifts were identified, including higher abundances of proteins associated with the production of extracellular polymeric substances. Confocal laser scanning microscopy indicated that EPS production was associated with greater cell aggregation when biomass was cultured at high-pressure. Changes in *Halanaerobium* central carbon metabolism under the same conditions were inferred from NMR and gas chromatography measurements, revealing large per-cell increases in production of ethanol, acetate and propanol and cessation of hydrogen production. These metabolic shifts were associated with carbon flux through 1,2 propanediol in response to slower fluxes of carbon through stage 3 of glycolysis. Together, these results reveal the potential for bio-clogging and corrosion (via organic acid fermentation products) associated with persistent *Halanaerobium* growth in deep, hydraulically fractured shale ecosystems, and offer new insights into cellular mechanisms that enable these strains to dominate deep shale microbiomes.

Deliverable 2. A paper detailing the results from this study has been submitted to *Applied and Environmental Microbiology*. Citation provided below:

Booker AE, Hoyt DW, Meulia T, Eder E, Nicora CD, Purvine SO, Daly RA, Moore JD, Wunch K, Pfiffner S, Lipton MS, Mouser PJ, Wrighton KC, and Wilkins MJ. Deep subsurface pressure stimulates metabolic flexibility in shale-colonizing *Halanaerobium*. Submitted to *Applied and Environmental Microbiology*. In review.

Additionally since the last report, the team's shale virus paper has been published in *Nature Microbiology*. Citation provided below:

Daly RA, Roux S, Borton MA, Morgan DM, Johnston MD, Booker AE, Hoyt DW, Meulia T, Wolfe RA, Hanson AJ, Mouser PJ, Sullivan MB, Wrighton KC, and Wilkins MJ (2018) Viruses

control dominant bacteria colonizing the terrestrial deep biosphere after hydraulic fracturing. *Nature Microbiology*. doi: 10.1038/s41564-018-0312-6

The deep terrestrial biosphere harbors a substantial fraction of Earth's biomass and remains understudied compared with other ecosystems. Deep biosphere life primarily consists of bacteria and archaea, yet knowledge of their co-occurring viruses is poor. Here, researchers temporally catalogued viral diversity from five deep terrestrial subsurface locations (hydraulically fractured wells), examined virus–host interaction dynamics and experimentally assessed metabolites from cell lysis to better understand viral roles in this ecosystem. Researchers uncovered high viral diversity, rivalling that of peatland soil ecosystems, despite low host diversity. Many viral operational taxonomic units were predicted to infect *Halanaerobium*, the dominant microorganism in these ecosystems. Examination of clustered regularly interspaced short palindromic repeats–CRISPR-associated proteins (CRISPR–Cas) spacers elucidated lineage-specific virus–host dynamics suggesting active in situ viral predation of *Halanaerobium*. These dynamics indicate repeated viral encounters and changing viral host range across temporally and geographically distinct shale formations. Laboratory experiments showed that prophage-induced *Halanaerobium* lysis releases intracellular metabolites that can sustain key fermentative metabolisms, supporting the persistence of microorganisms in this ecosystem. Together, these findings suggest that diverse and active viral populations play critical roles in driving strain-level microbial community development and resource turnover within this deep terrestrial subsurface ecosystem.

Mouser Lab (OSU-UNH)

Milestone 1. Characterization of intact polar lipids in MSEEL core and fluid samples

Mouser team had hoped to submit the manuscript below for review by the end of this quarter; however, the paper is still in the final stages of editing based on co-author feedback. The team expects to submit the paper for review by the end of January.

Microbial Membrane Lipids Show De Novo Ecosystem Transformation in Hydraulically Fractured Marcellus Shale, Andrea J. Hanson, Julius S. Lipp, Rebecca A. Daly, Julia M. Sheets, Susan A. Welch, Shikha Sharma, Timothy R. Carr, Michael R. Wilkins[4], Kelly C. Wrighton, David R. Cole, Kai-Uwe Hinrichs, Paula J. Mouser

Hydrocarbon extraction technologies utilizing hydraulic fracturing methods have unlocked deep subsurface environments that have remained sequestered from surface ecoystems for millions of years. Although recent metagenomic studies have established patterns of microbial succession and metabolic potential in the anaerobic, saline fluids produced by low-permeability hydrocarbon systems, the presence of microbial ecosystems indigenous to deep rock habitats and the basis for their physiological adaptations during natural gas well maturation are poorly described. Here, researchers surveyed deep terrestrial rock cores for signs viable life pre-hydraulic fracturing, and characterized intact polar lipids (IPLs) in fluids produced from a Marcellus Shale natural gas well in concert with mineralogical, geochemical, and metagenomic evaluations to understand microbial membrane acclimation within this engineered subterra. Limited evidence of ancient or modern biosignatures in 2 km deep rock cores combined with a diversity of bacterial and archaeal IPLs induced by drilling and well completion mark a distinct transition from a desolate deep terrestrial system to a biosphere that supports abundant microbial life. In contrast to metagenomic predictions, anionic and glycosylated IPL head groups dominated lipid signatures in the shale-produced fluids, with structures exerting an influence on membrane permeability, interactions with mineral surfaces, and cellular bioenergetics. Analysis shows IPLs materially contribute to

microbial membrane adaptation in response to salinity, temperature, and chemical conditions following energy extraction.

Milestone 2. Characterization of dehalogenation pathways in MSEEL fluid samples.

Evans is in the process of analyzing metagenome data and reconstruct pathways related to dehalogenation. She will finalize a manuscript associated with this data during Jan-March 2019 quarter, corresponding author Mouser with Evans first author.

Cole Lab (OSU)

Milestone 1. Complete analysis of trace metal composition of flowback fluid samples.

Role of Rock Chemistry and Mineralogy

Determining the minerals/organic matter (OM) that are solubilized during hydraulic fracturing and contribute most to elements observed in produced fluids remains elusive. Of particular concern to operators who work with hydraulically-fractured formations in the Appalachian basin are Ba and Sr, which foul equipment by precipitating as scale and present problems for disposal. One hypothesis suggests that calcite, OM, and clay minerals are potential contributors to such elements, including radium isotopes, which are daughters of uranium and thorium (Landis et al., 2018). Direct observations of the Lower Marcellus and associated formations (electron microscopy) along with bulk measurements XRD/XRF/QEMSCAN show that other mineral groups may also be important for releasing such elements.

Integrating input and flowback fluid analysis with whole core elemental and mineralogical analysis helps shed light on the source(s) of specific elements observed in produced water chemistries. This is especially useful when comparing two very different hydraulic fracturing targets—the carbonate-rich Point Pleasant and silicate-rich Lower Marcellus. The Cole group has had the opportunity to sample 2 wells for input and flowback fluids from each of these formation targets, allowing some inferences about water-rock interactions that result from hydraulic fracturing at these sites. For example, U concentration is significantly greater (as measured with XRF in Lower Marcellus core) as compared to the 3 Gulfport Point Pleasant core.

For example, both Ba and Sr are reported in high concentrations relative to natural waters from many hydraulically-fractured lateral wells sampled in the Appalachian Basin. Focusing on a Lower Marcellus core sample from MSEEL well MIP 3H (depth 7543′), XRF elemental data show Ba >> than Sr (by about 3-fold) with a concentration of about 1000 ppm (see Cole group Q3 report, 2018). Barium in the overlying Middle Marcellus core (depth 7509′) also is nearly 1000 ppm Ba, with about a 7-fold higher concentration than strontium. **Point Pleasant core data** essentially show the reverse trend, with Sr >> Ba (Sr concentration about 1000 ppm), and ranging from about 3 to 9-fold greater than Ba.

Barite is identified in powder XRD analysis of the same core sample **(Figures 3.5 and 3.6**), and QEMSCAN mineral mapping reveals a Ba-rich phase as part of unclassified pixels (**Figure 3.7, see caption**). Spectral overlap between Ti and Ba requires verification of clay-sized grains with EDX spot analysis. This analysis along with BSE imagery reveals complex mineralogy in the clay fraction, including clay-sized barium sulfate, zinc sulfide, REE phosphate, and a uranium/titanium bearing phase (**Figure 3.8**). The latter is observed in close association with framboidal pyrite, as discrete particles within the rock matrix, and within OM. Slightly elevated trace concentrations of U in the XRF measurements of the Lower Marcellus may reflect the U-Ti phase observed in the clay fraction

* Landis, Sharma, Renock, and Niu, (2018), Rapid desorption of radium isotopes from black shale during hydraulic fracturing. 1. Source phases that control the release of Ra from Marcellus shale. Chem. Geol. 496, 1-13.

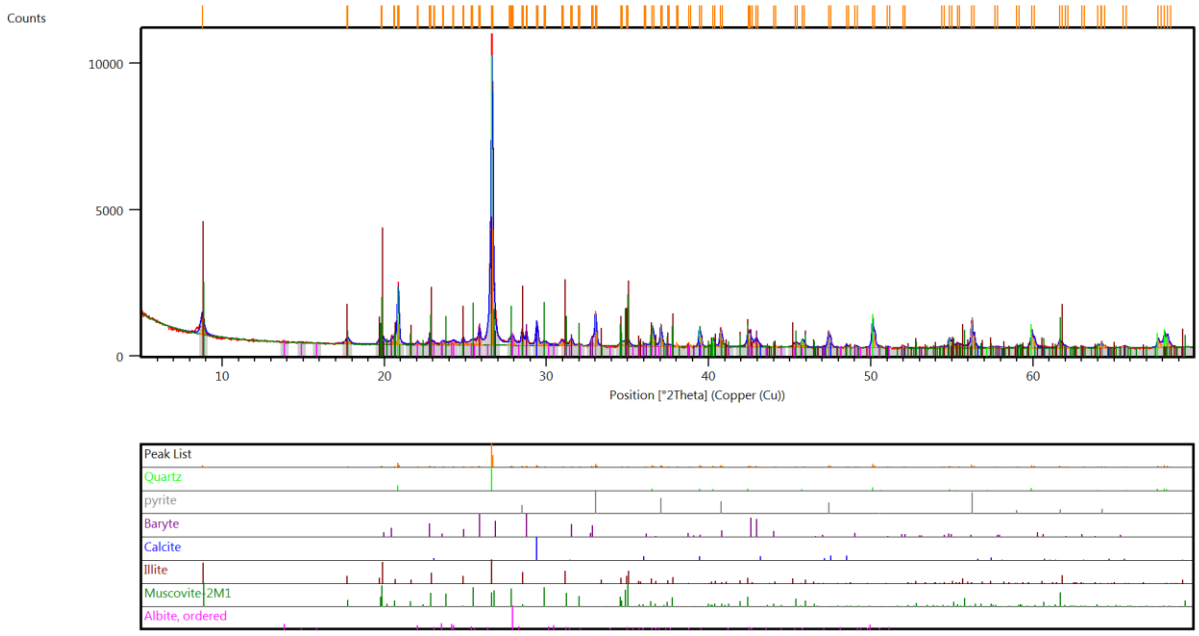

Figure 3.5. Mineral identification with powder XRD of Lower Marcellus core, depth 7543'. Upper diagram shows experimental scan (red) with colored lines representing minerals matched to those lines superimposed. Phase ID is shown in lower diagram by peak matching the red experimental list with line locations and relative intensities of powder patterns available in the PDF 4+ mineral database.

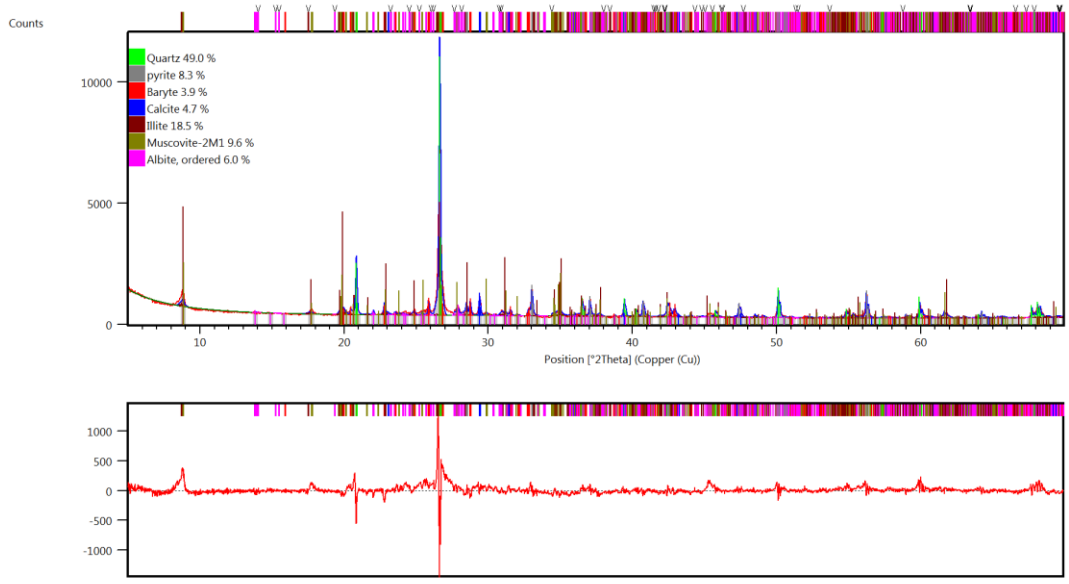

Figure 3.6: Quantification of minerals for Lower Marcellus core depth 7543' with Rietveld refinement (upper diagram) of the dataset shown in Figure X. Difference plot (lower diagram) is produced by subtracting the calculated scan (blue) from experimental scan (red). Illitic clay and muscovite are underdetermined by the model, as shown by peak residuals above the zero intensity line in the lower diagram (see, for example, illitic clay/muscovite residual intensities at about 8.8 and 17.7 degrees 2-theta).

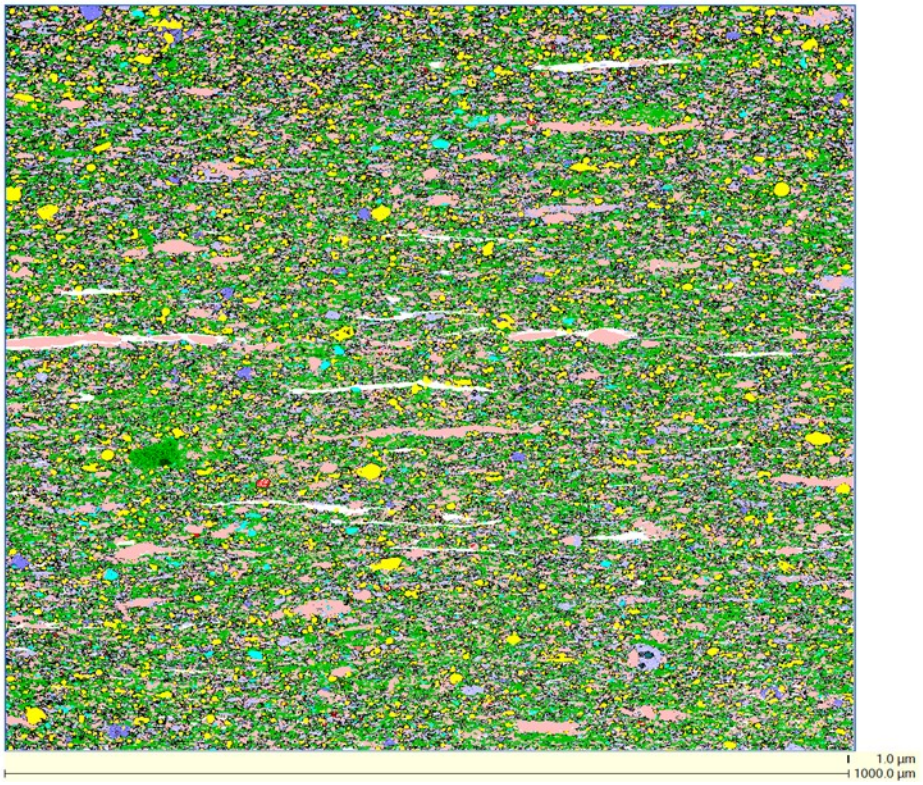

Figure 3.7: QEMSCAN mineral map of 1 mm^2 region of Lower Marcellus, depth 7543'. Mineral composition includes illitic clay (green pixels, 25.7 %); quartz (pink, 25.2 %); unclassified pixels (black, 22.5 %); calcite (lavender, 10.3 %); pyrite (yellow, 8.8 %); albite (cyan, 1.6 %); OM (white 3.4 %), gypsum/anhydrite (purple, 1 %), dolomite (dark lavender, 0.7 %). Remaining < 1% includes small quantities of mica (dark green); titania (red); Ca-phosphate (bright pink), and K-feldspar. EDX spot analysis is required to verify the clay fraction mineralogy. Micrometer-sized barite, ZnS (sphalerite), REE phosphate, and the U-Ti phase are part of the unclassified pixels (black) that cannot be resolved with QEMSCAN mineral mapping.

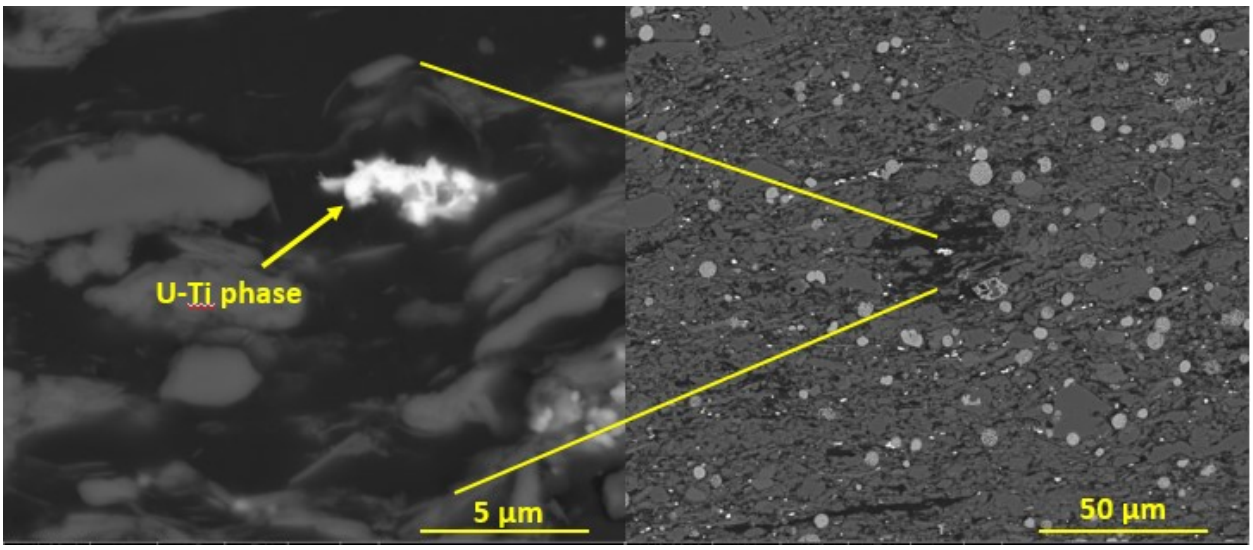

Figure 3.8: BSE imagery of Lower Marcellus, depth 7543' showing complex details in the matrix clay fraction of this core. Bright phases that are 1s of µm in length scale include pyrite, barite, REE phosphates, sphalerite (ZnS) and a U-Ti phase, as identified by EDX spot analysis. The uranium-bearing phase is arrowed and a lower magnification of the region interrogated is also shown (right) for context.

Deliverable 1. Compilation of the flowback fluid chemistry.

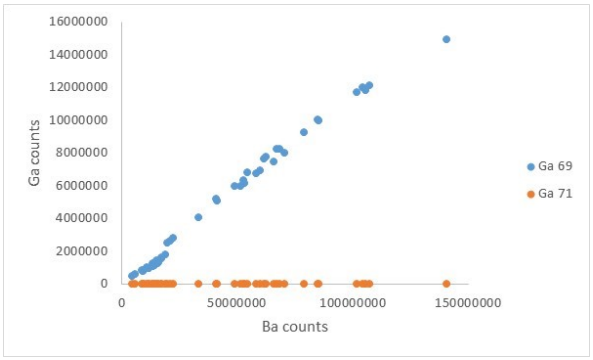

Flowback Chemistry

All of the flowback fluid samples that were received by the Cole group have been analyzed for selected trace metals using a Quadrapole ICP-MS and the results of these analysis are currently being calculated and compiled. Analysis of these complex brines is analytically challenging because the elevated levels of Sr and Ba in solution can form complex polyatomic species in the plasma in the form of metal hydrides, oxides, hydroxides, argides, chlorides or other species, as well forming doubly charged ions, which can result in the generation of isobaric interferences on the masses of interest for other elements. These interferences are particularly problematic for interpreting data for the transition and rare earth elements. Examples of these analytical interferences are depicted in Figure 3.9.

Analysis of all the data generated from these preliminary analysis will be carefully reviewed, and if needed samples will be analyzed again using one (or both) of the other two ICP-MS instruments available. One is equipped with a collision cell that allows for additional gases to minimize oxide interferences, the other can operate in low, medium or high resolution modes to focus on the narrow plateau on the peak generated by the element of interest. The tradeoff between these systems and the Quadrapole ICP-MS, is better removal of interfering polyatomic isobars, but also poorer detection limits for most elements. These two ICP-MS instruments have been largely unavailable in the last quarter (Oct-Dec 2018) due to ongoing repairs of the buildings ventilation and airhandlers.

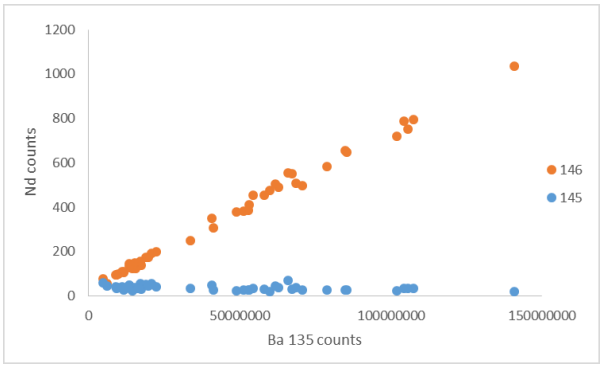

Figure 3.9: Examples of isobaric interferences in mass spectrometry. Left) signal intensity for ^{69}Ga and ^{71}Ga. The elevated signal for ^{69}Ga is probably a doubly charged ^{138}Ba ion forming in the plasma, resulting in a m/z of 69. The expected ratio for ^{69}Ga:^{71}Ga is ~ 3:2. Right) signal intensity for ^{145}Nd and ^{146}Nd. The strong correlation between Ba and ^{146}Nd suggests a polyatomic species with mass 146, presumably ^{130}Ba^{16}O. These interferences can be estimated by analyzing numerous standards with and without these elements and determining correction factors for the elements of interest.

In spite of these analytical difficulties, trace metal data has been compiled for many elements of interest in the fluids from the MIP 3H and 5H wells. Some of the elements measured (such as Li, Rb and Cs) generally follow the same trends as other salts, while others, such as Mo, W, and Pb either showed little change or decreasing concentrations over time.

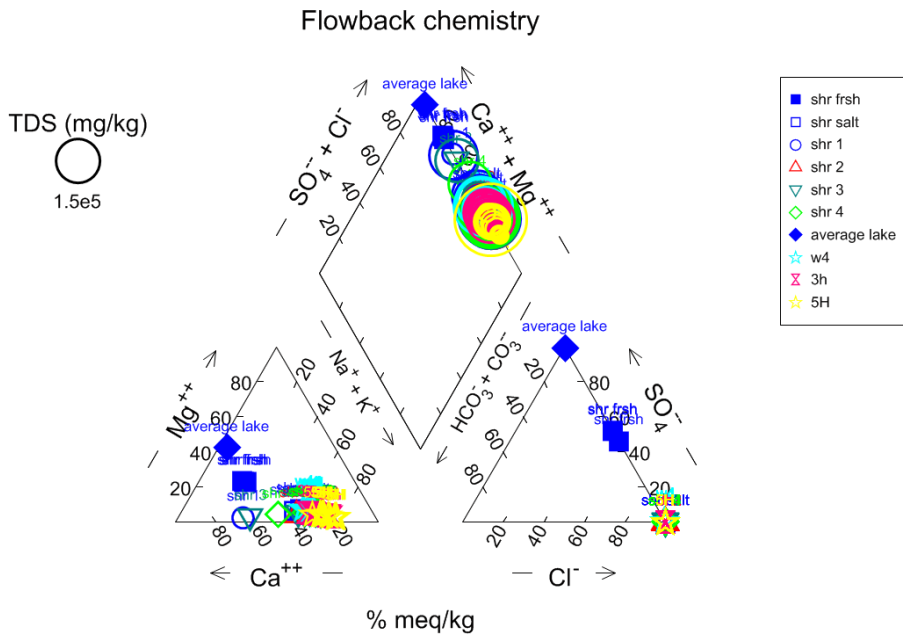

Figure 3.10: Piper diagram of flowback fluids and input fluids from two sites in the Utica-Pt. Pleasant in eastern Ohio (W4 and Shr 1_4) and the MIP 3H and 5H.

These fluids can be described as Na-Ca-Cl brines with total dissolved salt (TDS) concentrations ranging from approximately 40 to 250 g/l salt (Figure 3.6). In general TDS of flowback composition from these three sites follow similar trends, increasing rapidly in the first few weeks of flowback, and then much more slowly over time. The one exception to this trend was from the MIP 5H well that exhibited a two fold increase in TDS for the brine sample collected at day 462 compared to the samples collected in the months before and after. Most of the major elements in these brines (Na, Ca, Cl, Br, etc) follow similar trends, or have similar ion ratios in solution, suggesting that they behave conservatively and are controlled by similar geochemical processes (Figure 3.11). For example, there is a strong correlation between Cl and Br suggesting that they behave conservatively, and the similarity amongst the brines from all the wells suggests that there was no appreciable contribution of salt from halite dissolution, since Br is excluded from the halite structure. Other elements, such as K, which readily reacts between the fluids and ion exchange sites on clays, generally exhibit conservative behavior within for an individual site, but show large variations between the three well pads, suggesting that differences in geochemical and mineralogical composition of the formation exerts control on the fluid chemistry.

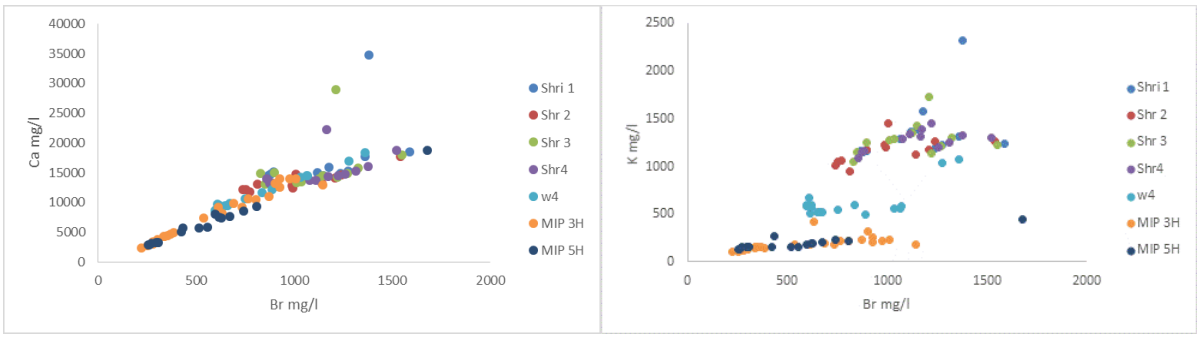

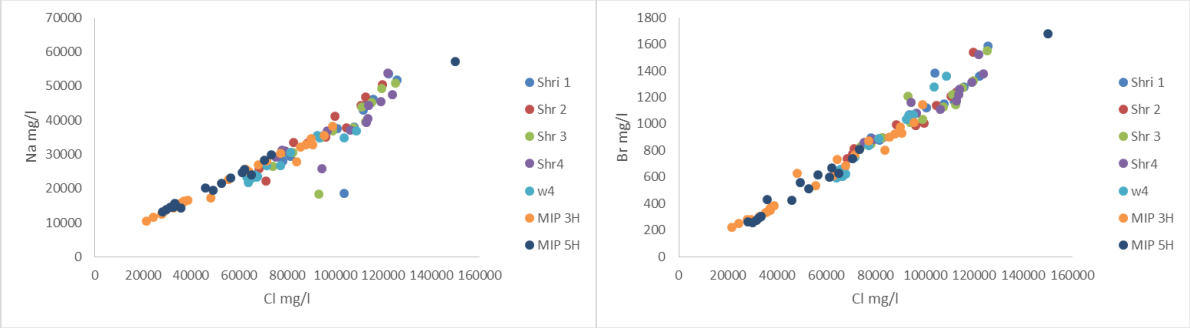

Figure 3.11: Cross plots of Na vs Cl, Br vs Cl, Ca vs Br, and K vs Br for brine samples from the seven wells. The strong correlation between these elements suggest similar geochemical processes control their distributions in the brines.

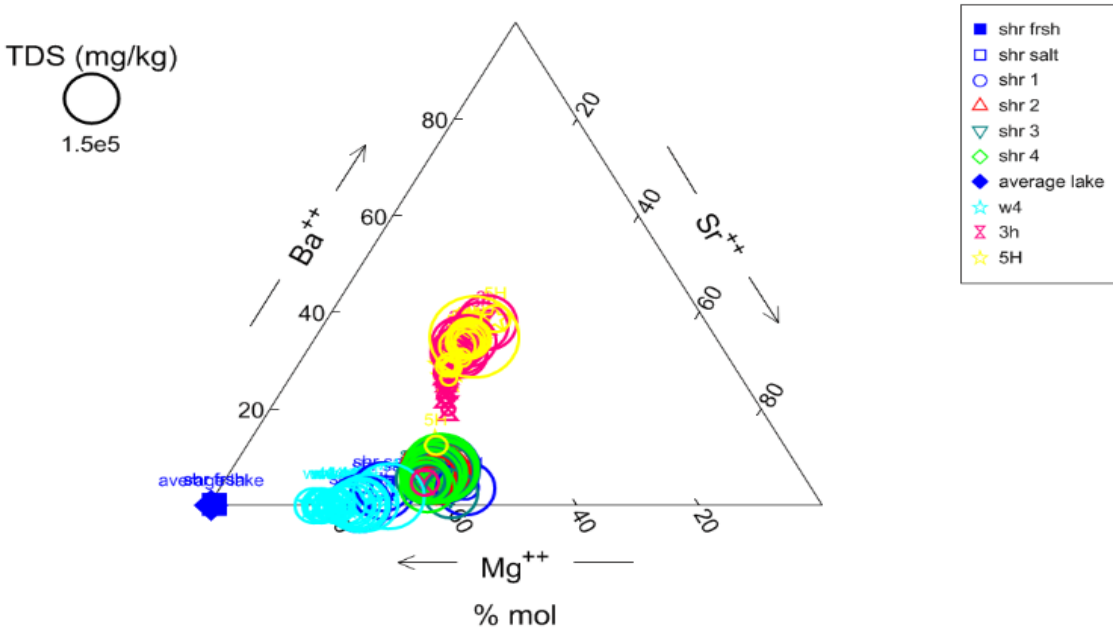

Although the concentrations of most major elements in the fluids are similar, the concentrations of Sr and Ba in the fluids from the three sites are remarkably different, and these differences are the result of differences in both the lithology and the input fluids. The highest levels of Ba (up to ~ 10 g/l) were measured in brines from the MSEEL site (Figure 3.12), and the brines from the MSEEL fluids have Ba:Sr ratios of approximately 2:1 (wt:wt). In comparison, the geochemical and mineralogical analysis of the rocks near the MSEEL target show Ba in excess of 1 g/kg and Ba:Sr ratios ranging from approximately 3:1 to 7:1 with abundant barite identified by both SEM and XRD (Figure 3.13). Sr concentrations in flowback fluids from the Utica-Point Pleasant Shale sites are approximately two fold higher than those in the MSEEL fluids, reflecting higher Sr

Figure 3.12: Ternary diagram showing the differences in the MSEEL, W4 and Shr locations.

concentrations in the rock and a more carbonate rich lithology. Celestite ($SrSO_4$) or barite/celestite, strontianite ($SrCO_3$) (often observed as thin rims on carbonate fossils), or Sr-rich phosphate phases are frequently observed in the Utica-Point Pleasant Shale. The most striking difference however was observed for the Ba concentrations in the W4 well. The input fracking fluid for this site had elevated SO_4^{2-}, resulting in precipitation of barite/celestite in the fluids and lower Ba and Sr in solution.

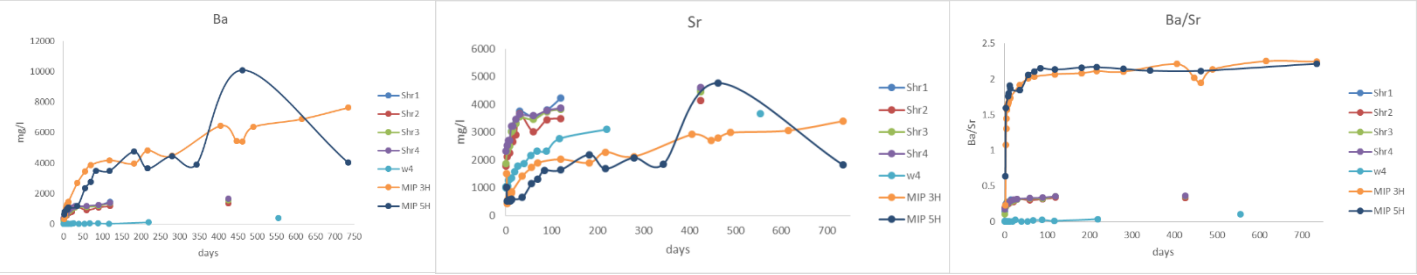

Figure 3.13: Sr, Ba and Ba/Sr ratios in flowback fluids from the seven wells sampled.

Deliverable 2. Produce a draft of a manuscript comparing geochemistry of flowback fluids between Utica and Marcellus wells.

SAW, JMS, and DRC are drafting a paper comparing the geochemistry of flowback fluids from two locations in eastern Ohio (Utica-Point Pleasant Shale) to the geochemistry of fluids from the MSEEL site. The flowback fluids from these three locations (seven wells in total) have remarkably similar composition in spite of the different lithologies, and have a composition that is distinct from, though affected by, the composition of the input fluids (Figures 3.6 through 3.9 constitute a portion of the figures used in the paper).

Darrah Lab (OSU)

Milestone 1. Characterization of remaining mineral samples from cores.

A total of nine rock samples and nine fluid inclusion samples have been analyzed for noble gas composition (reported data ranges with detectable concentrations, but includes He, Ne, and Ar, abundances and isotopic compositions). Krypton and xenon concentrations and isotopic analyses were completed on six samples in total (as determined by method detection limits). Data reports for each sample also includes total pressure and bulk gas geochemistry (C_1-C_5, CO_2, N_2, H_2.

Deliverable 1. Data report for remaining noble gas and hydrocarbon composition of fluid inclusions.

A paper is in preparation that summarizes these noble gas data from the rock characterization.

Milestone 2. Compile information for a publication from fluid (gas and water) samples through time.

Characterization of water and gas samples for noble gas (He, Ne, Ar, Kr, and Xe), fixed gas (N_2, H_2, CO_2) and hydrocarbon gas (C1-C5, C6+) composition (11 samples remain).

Data report for remaining noble gas, hydrocarbon, and fixed gas measurements. The data report for produced water (n=49 samples) and gas samples (n=14 samples) has now been finalized. This includes the completion of 63 samples for noble gas isotope (He, Ne, Ar, Kr, and Xe) and bulk gas geochemistry (C_1-C_5, CO_2, N_2, H_2).

This work represents the funded portion of the MSEEL project and brings the total of noble gas samples to n=89 combined natural gas (n=40) and produced water (n=49) samples that have been analyzed and reported.

Deliverable 2. Submit manuscript about changes in the hydrocarbon, fixed, and noble gas composition throughout time.

A second paper is being prepared that summarizes and interprets all of the gas and fluid noble gas isotope and geochemistry data.

Products

Sharma's Lab

PUBLICATIONS & PRESENTATIONS

Research Papers

1. Akondi, R., Sharma, S., Trexler, R. V., Mouser, P., & Pfiffner, S. (2019). Microbial Lipid Biomarkers Detected in Deep Subsurface Black Shales. Environmental Science: Processes & Impacts. https://doi.org/10.1039/C8EM00444G
2. Agrawal, V. & Sharma, S. 2018. Improved Kerogen models for determining hydrocarbon potential and thermal maturity of shales. *Scientific Reports* 8:17465 | DOI:10.1038/s41598-018-35560-8
3. Pilewski. J, Sharma, S., Agrawal, V., Hakala,A., Stuckman, M., 2018. Effect of Maturity and Mineralogy on Fluid-Rock reactions in the Marcellus Shale. Environmental Science: Processes & Impacts (accepted)
4. Phan T., Hakala A., Lopano C. and Sharma S. 2018. Rare earth elements and radiogenic Sr isotopes in carbonate minerals reveal diagenetic influence in shales and limestones in the Appalachian Basin. Chemical Geology (accepted)
5. Borton, M. A., et. al., 2018. Comparative genomics and physiology of the genus Methanohalophilus, a prevalent methanogen in hydraulically fractured shale. Environmental Microbiology, 20 (12)-4596-4511 https://doi.org/10.1111/1462-2920.14467.
6. Borton, M. A., et. al., 2018. Coupled laboratory and field investigations resolve microbial interactions that underpin persistence in hydraulically fractured shales. Proceedings of the National Academy of Sciences, 115.28 (2018): E6585-E6594.
7. Moore, J., Xiong, W., Lopano, C., Phan, T., Vankeuren, A., Sharma, S., ... & Hakala, A. 2018. Bench-Top Experiments Evaluating Simulated Hydraulic Fracturing Fluid Interactions with Marcellus Shale Core. Proceedings URTeC 2018; 852-862

Presentations

8. Agrawal, V., Sharma, S., 2018. Should the physicochemical properties of shale and kerogen modelled using kerogen 'type'? Geological Society of America (GSA), Annual meeting, 4-7 Nov, Indianapolis, Indiana.
9. Sharma S, John P, Agrawal V, Hakala A, Stuckman M. 2018. Understanding fluid-rock interactions in shales using high temperature-pressure reactors. Geological Society of America (GSA), Annual meeting, 4-7 Nov, Indianapolis, Indiana.

10. Akondi R., Sharma S. 2018. Changes in Microbial Lipid Biomarkers Associated with Storage Conditions in Subsurface Shale Cores. AGU's Fall Meeting 2018, 10-14 December, Washington, D.C. 4.
11. Akondi R., Sharma S. 2018. Assessing the Effects of Sampling and Long Term Storage on Microbial Lipid Biomarker Distribution in Deep Subsurface Marcellus Shale, Appalachian Basin. Geological Society of America (GSA), Annual meeting, Indianapolis, Indiana. 5
12. Agrawal, V., Sharma, S., 2018. New models for determining thermal maturity and hydrocarbon potential in Marcellus Shale. Eastern Section AAPG 47th Annual Meeting in Pittsburgh, WV

Wrighton's Lab (OSU-CSU); Wilkins Lab (OSU-CSU)

Borton MA, Daly RA, O'Banion B, Hoyt DW, Marcus DN, Welch S, Hastings SS, Meulia T, Wolfe RA, Booker AE, Sharma S, Cole DR, Wunch K, Moore JD, Darrah TH, Wilkins MJ, and Wrighton KC (2018) Comparative genomics and physiology of the genus Methanohalophilus, a prevalent methanogen in hydraulically fractured shale. *Environmental Microbiology*. doi: 10.1111/1462-2920.14467

Booker AE, Hoyt DW, Meulia T, Eder E, Nicora CD, Purvine SO, Daly RA, Moore JD, Wunch K, Pfiffner S, Lipton MS, Mouser PJ, Wrighton KC, and Wilkins MJ. Deep subsurface pressure stimulates metabolic flexibility in shale-colonizing *Halanaerobium*. Submitted to *Applied and Environmental Microbiology*. In review.

Daly RA, Roux S, Borton MA, Morgan DM, Johnston MD, Booker AE, Hoyt DW, Meulia T, Wolfe RA, Hanson AJ, Mouser PJ, Sullivan MB, Wrighton KC, and Wilkins MJ (2018) Viruses control dominant bacteria colonizing the terrestrial deep biosphere after hydraulic fracturing. *Nature Microbiology*. doi: 10.1038/s41564-018-0312-6

Mouser's Lab

Peer Reviewed Publications associated with MSEEL:

Akondi R. Sharma S, Trexler R, **Mouser PJ**, Pfiffner S. Microbial Lipid Biomarkers Detected in Deep Subsurface Black Shales, (2018). *Environmental Sciences: Processes & Impacts*. Available in advance at doi: 10.1039/C8EM00444G.

Three papers are in preparation that involve MSEEL related samples/topics that are planned for submission in Jan - March timeframe.

Darrah's Lab (OSU)

A paper is in preparation that summarizes these noble gas data from the rock characterization. A second paper is being prepared that summarizes and interprets all of the gas and fluid noble gas isotope and geochemistry data.

Plan for Next Quarter

Work to wrap up the results of MSEEL and prepare to extend to subsequent MSEEL wells.

Topic 4 – Environmental Monitoring – Surface Water & Sludge

Approach

Almost three years into the post completion part of the program, the produced water and solid waste component of MSEEL has continued to systematically monitor changes in produced water quality and quantity. During year one of the study, hydraulic fracturing fluid, flowback, produced water, drilling muds and drill cuttings were characterized according to their inorganic, organic and radio chemistries. In addition, surface water in the nearby Monongahela River was monitored upstream and downstream of the MSEEL drill pad. Toxicity testing per EPA method 1311 (TCLP) was conducted on drill cuttings in both the vertical and horizontal (Marcellus) sections to evaluate their toxicity potential. Sampling frequency has been slowly scaled back following well development. Table 4.2 shows an "X" for sample collection dates. Wells 4H and 6H were brought back online in late 2016. Other blank sample dates in Table 4.2 indicate that samples were not collected, due to lack of availability of produced water from the well(s).

Table 4.2: MIP sampling events are indicated with an "X".

Year	2015			2016												
Day/Month	10-Dec	17-Dec	22-Dec	6-Jan	20-Jan	3-Feb	2-Mar	23-Mar	20-Apr	18-May	2-Jul	17-Aug	21-Jun	19-Oct	16-Nov	14-Dec
3H	X		X	X	X	X		X	X	X	X	X	X	X		X
4H															X	X
5H	X	X	X	X	X	X	X	X	X	X	X	X	X	X	X	
6H															X	X

Year	2017									2018					
Day/Month	13-Jan	14-Feb	13-Mar	7-Apr	5-May	12-Jul	20-Dec	3-Nov	20-Dec	22-Jan	23-Feb	16-May	2-Aug	16-Oct	15-Dec
3H	X	X	X	X	X	X	X	X	X	X	X	X	X		X
4H	X	X	X	X	X					X	X	X	X	X	X
5H		X			X				X	X		X		X	X
6H	X	X	X	X	X							X	X		

Results & Discussion

Trends in produced water chemistry

Major ions

While makeup water was characterized by low TDS (total dissolved solids) and a dominance of calcium and sulfate ions, produced water from initial flowback is essentially a sodium/calcium chloride water (Figure 4.1). While produced water TDS (total dissolved solids) increased by an order of magnitude from initial flowback to the present. The ionic composition of produced water changed very little through 1101 days post completion. Produced water TDS was affected by shut-in/turn-in cycles at individual wells. For example, upon turn-in TDS was invariably very low but reached pre-shut-in concentrations within a month. MIP 3H was shut-in sometime after day 966 and turned back in just prior to sampling on day 1101. While concentrations are magnitudes lower, the proportion of ionic compounds is consistent with previous samples (

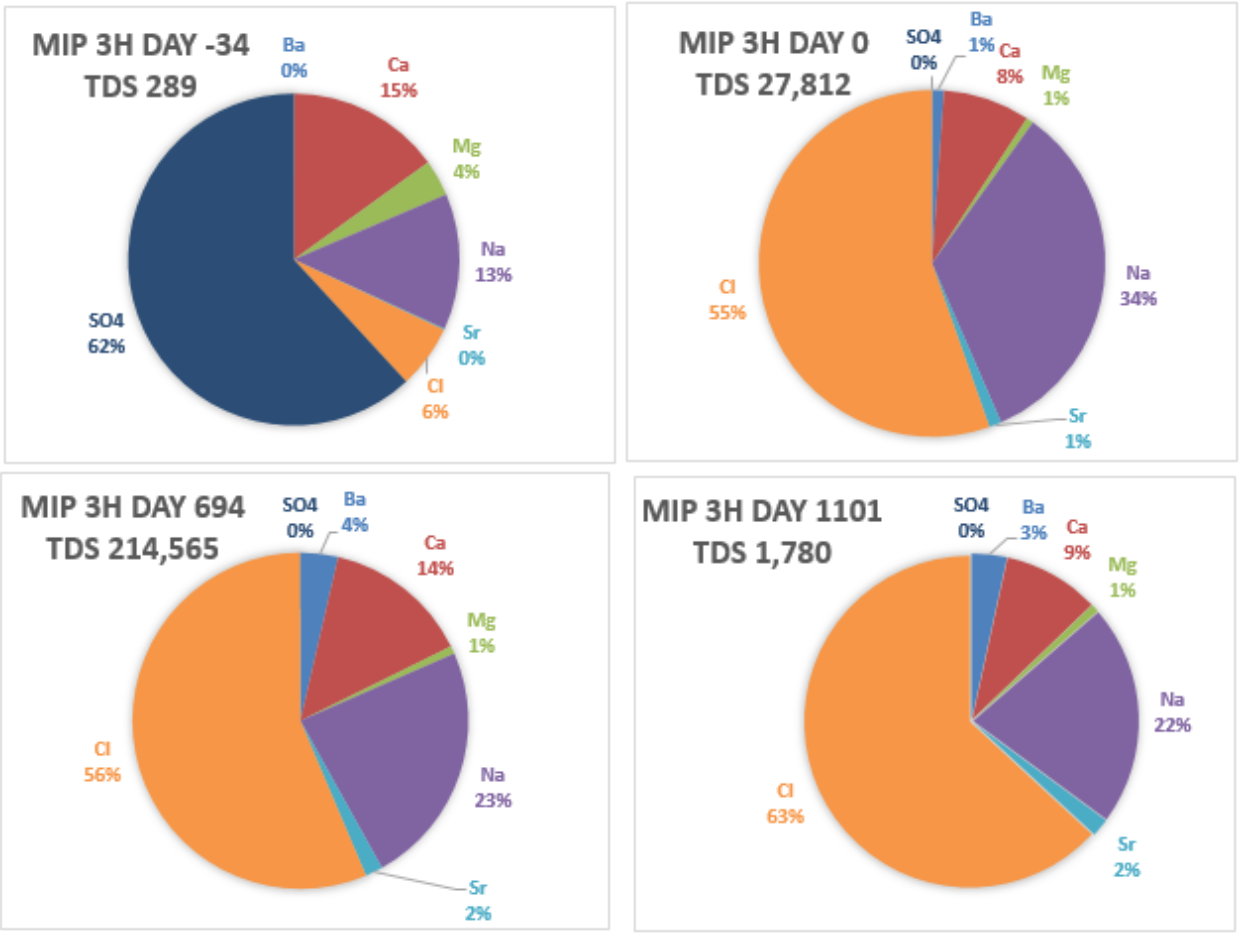
MIP 3H DAY -34
TDS 289
Ba 0%
Ca 15%
Mg 4%
Na 13%
Sr 0%
Cl 6%
SO4 62%
MIP 3H DAY 0
TDS 27,812
SO4 0%
Ba 1%
Ca 8%
Mg 1%
Na 34%
Sr 1%
Cl 55%
MIP 3H DAY 694
TDS 214,565
SO4 0%
Ba 4%
Ca 14%
Mg 1%
Na 23%
Sr 2%
Cl 56%
MIP 3H DAY 1101
TDS 1,780
SO4 0%
Ba 3%
Ca 9%
Mg 1%
Na 22%
Sr 2%
Cl 63%

Figure 4.1).

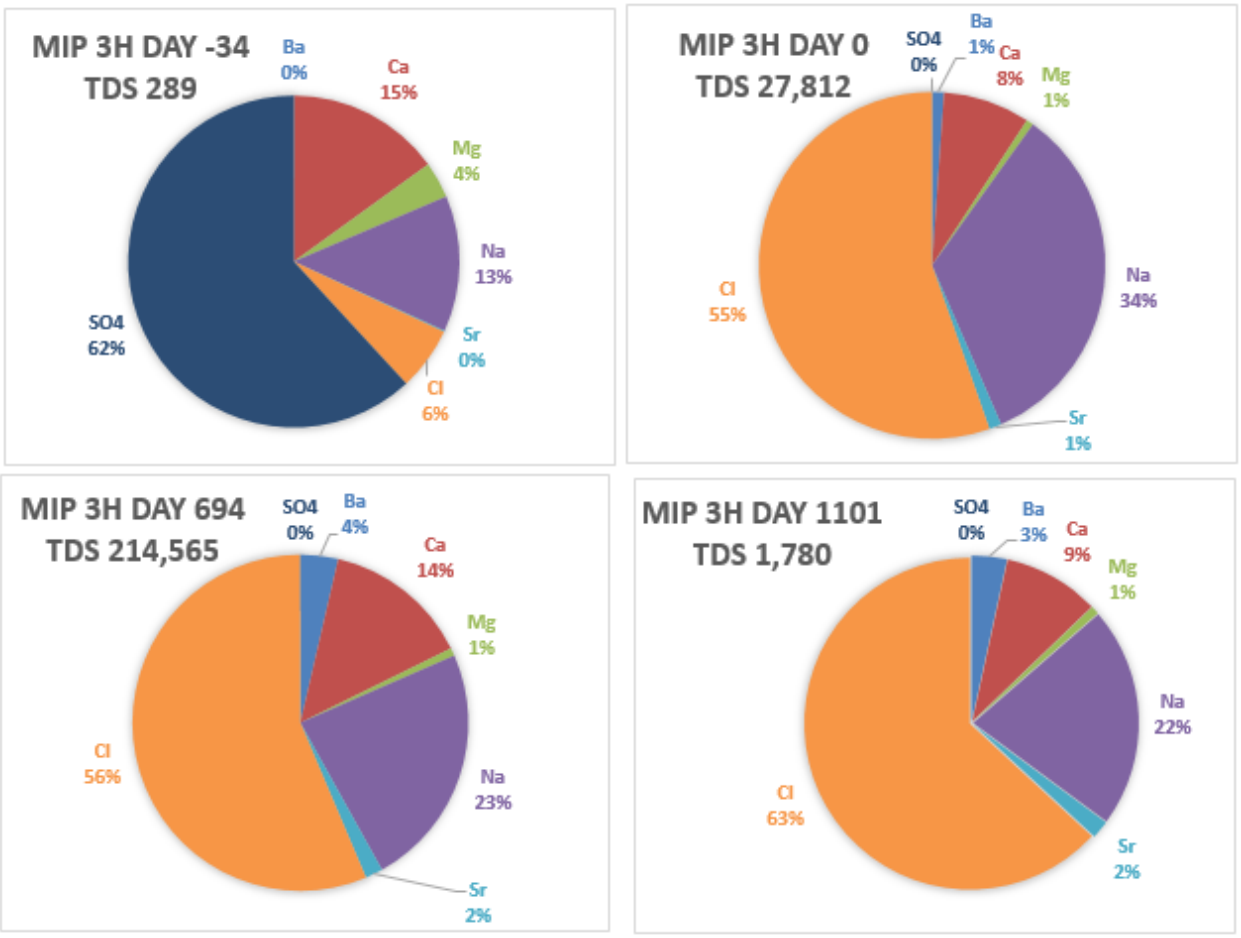

Figure 4.1: Changes in major ion concentrations in produced water from well MIP 3H. From left to right the charts represent makeup water from the Monongahela River, produced water on the first day of flowback and produced water on the 1101th day post completion.

In wells 3H and 5H, TDS increased rapidly over the initial 90 days post completion while TDS stabilized between 100,000 and 200,000 mg/L through day 1101(3H) (Figure 4.2). Note that 3H and 5H were both shut-in near day 966 and brought back online prior to sampling on day 1101.

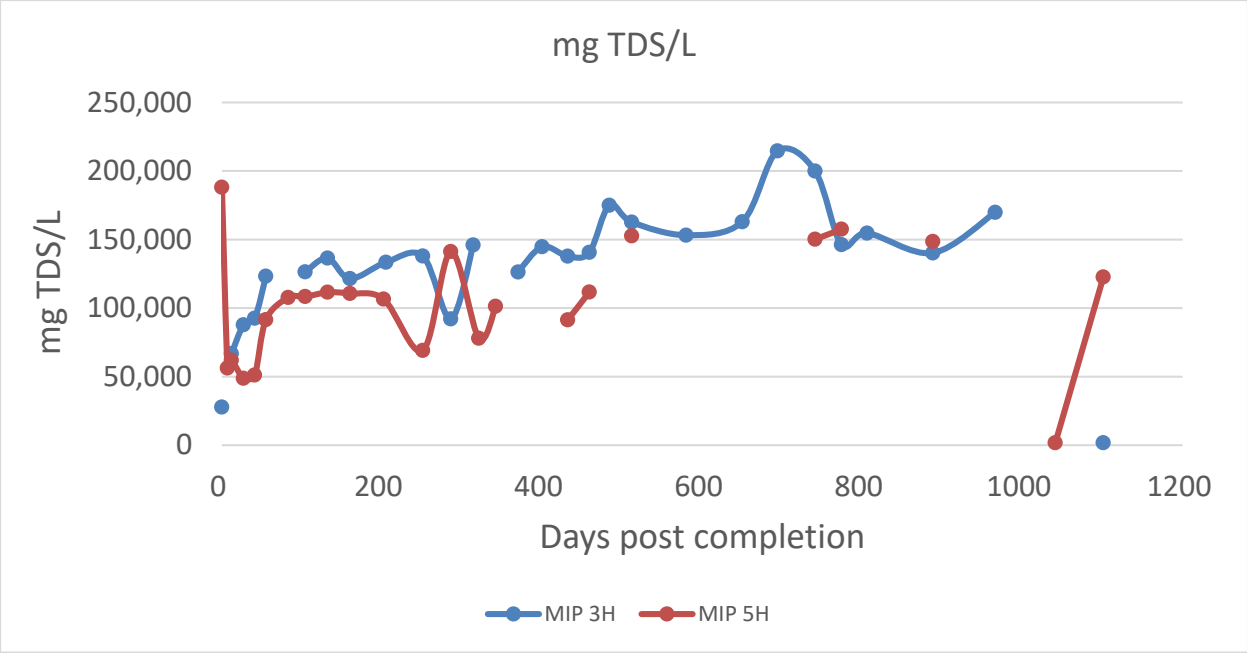

Figure 4.2: Changes in produced water TDS sdc (sum of dissolved constituents) through the first 1101 days post completion (3,5H).

The older 4H and 6H wells offer insight into the longer-term TDS trend. Those wells only came back on line during this quarter after a shut-in period of 315 days and those results vary but they are much lower than the current values for wells MIP 3H and 5H. Both 4H and 6H were shut down during late 2017. TDS was very low at MIP 4H during the first sampling event of early 2018. Calculated TDS was 2,455 mg/L and lab reported TDS was 2,300 mg/L. A similarly low TDS trend was noted when well 4H went back online around 1,793 days post-completion (after being shut-in for 315 days) and again when 6H went online around day 2,417 A rise in TDS subsequently follows the initial return to online status with TDS on an upward trend, reaching around 140,000 for MIP 4H and 160,000 for 6H (Figure 4.3).

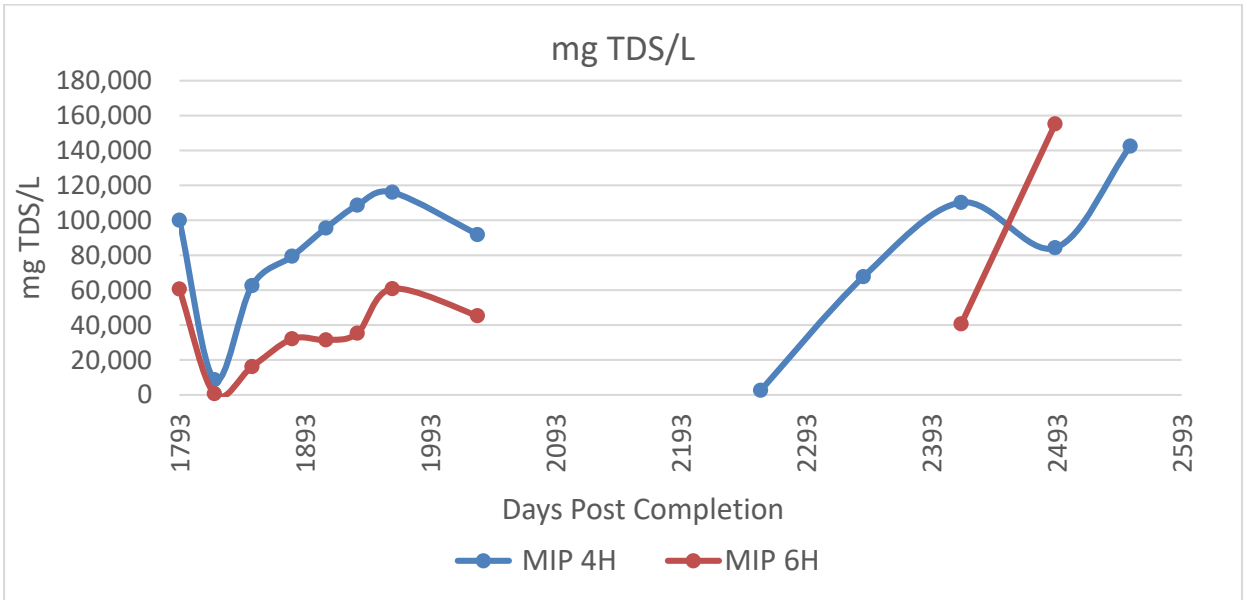

Figure 4.3: Changes in produced water TDS sdc (sum of dissolved constituents) through the days 1793 to 2552 post completion (4,6H).

Water soluble organics

The water soluble aromatic compounds in produced water: benzene, toluene, ethylbenzene and xylene were never high. With two exceptions at post completion day 321 and 694, benzene has remained below 30 µg/L (Figure 4.4). This seems to be a characteristic of dry gas geologic units. After five years, benzene has declined below the drinking water standard of 5 µg/L.

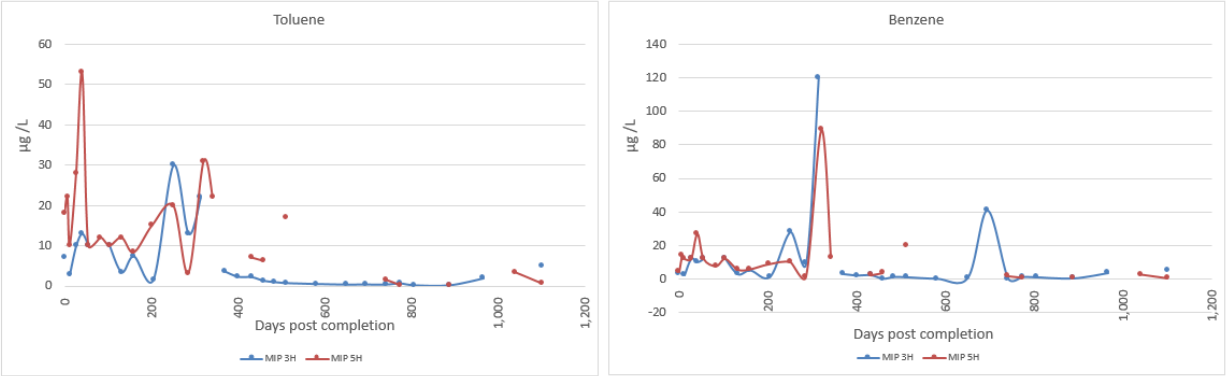

Figure 4.4: Changes in benzene and toluene concentrations. The figure shows data from well both 3H and 5H.

Radium isotopes

The radiochemical concentrations were determined by Pace Analytical in Greensburg PA, a state certified analytical lab. Radium concentrations generally increased through 800 days post completion at wells MIP 3H and 5H. Maximum levels of the radium isotopes reached about 20,000 pCi/L at the unchoked 3H well and about half that amount at 5H (Figure 4.5).

Radioactivity in produced water

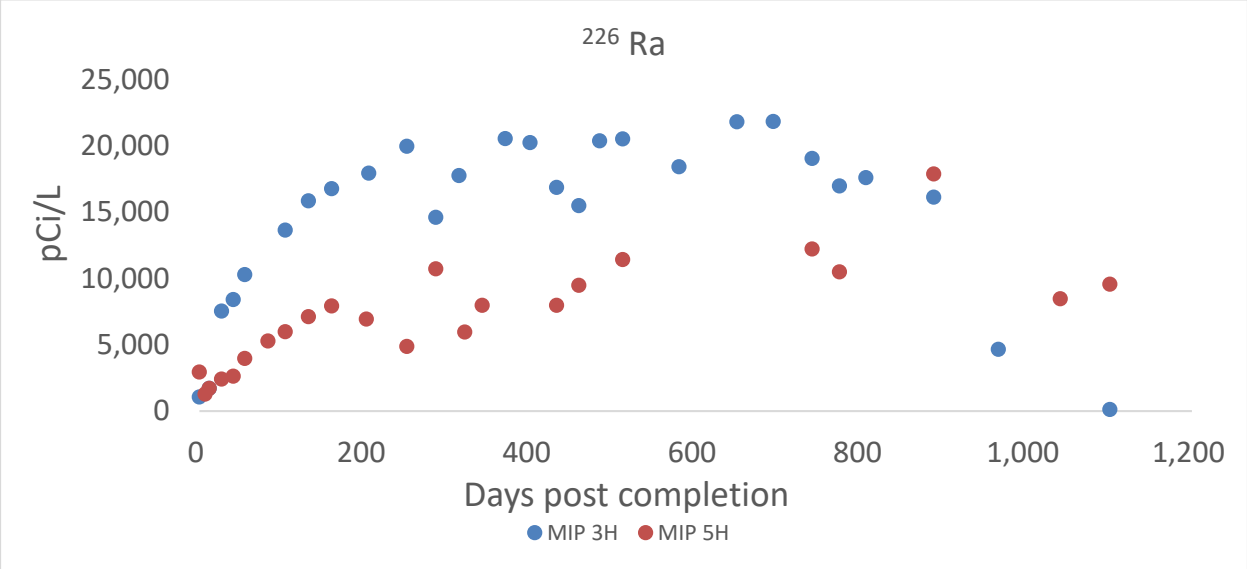

Figure 4.5: The radium isotopes are plotted against days post well completion. Well 5H was choked periodically. It produced less water and lower concentrations of radium.

Radium concentrations at wells 4H and 6H were below 9,000 pCi/L during all sampling periods. Both wells were choked at day 1963. Well 4H was reopened at day 2225, radium was 58 pCi/L on the first sampling after the reopening and 3719 pCi/L at day 2257, a month later (Figure) peaked at 5,127 pCi/L then returned to 3,892 pCi/L. Additional data is needed to capture long-term trends.

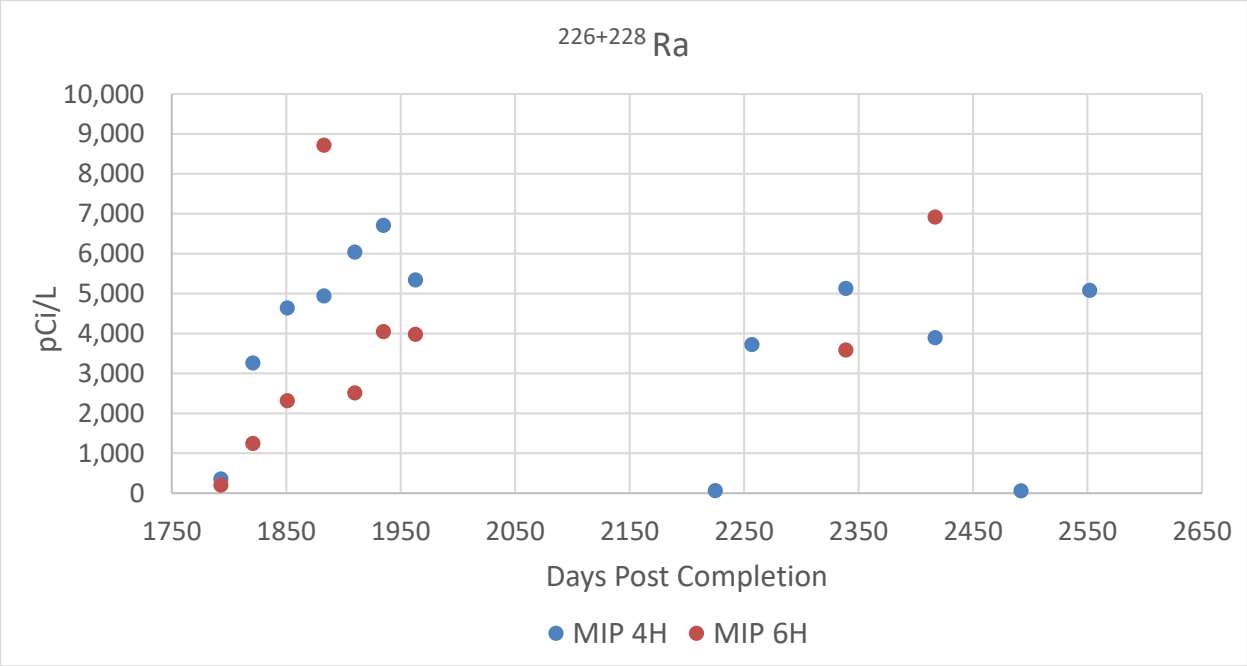

Figure 4.6: The radium isotopes are plotted against days post well completion. Well 4H and 6H were choked at day 1963. At day 2225, 4H was reopened showing a value of 58 pCi/L.

Figure 4.6 and 4.8 show the relationship between gross alpha and ^{226}Ra at 3H and 5H.

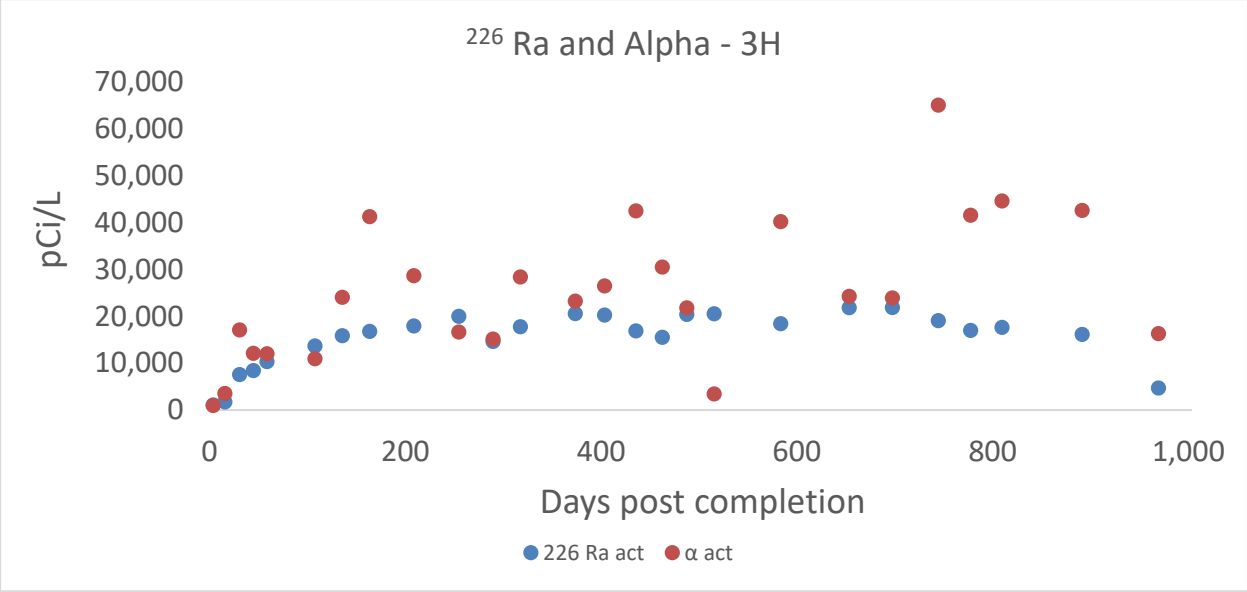

Figure 4.6: The relationship between gross alpha and ^{226}Ra as a function of time post completion at 3H.

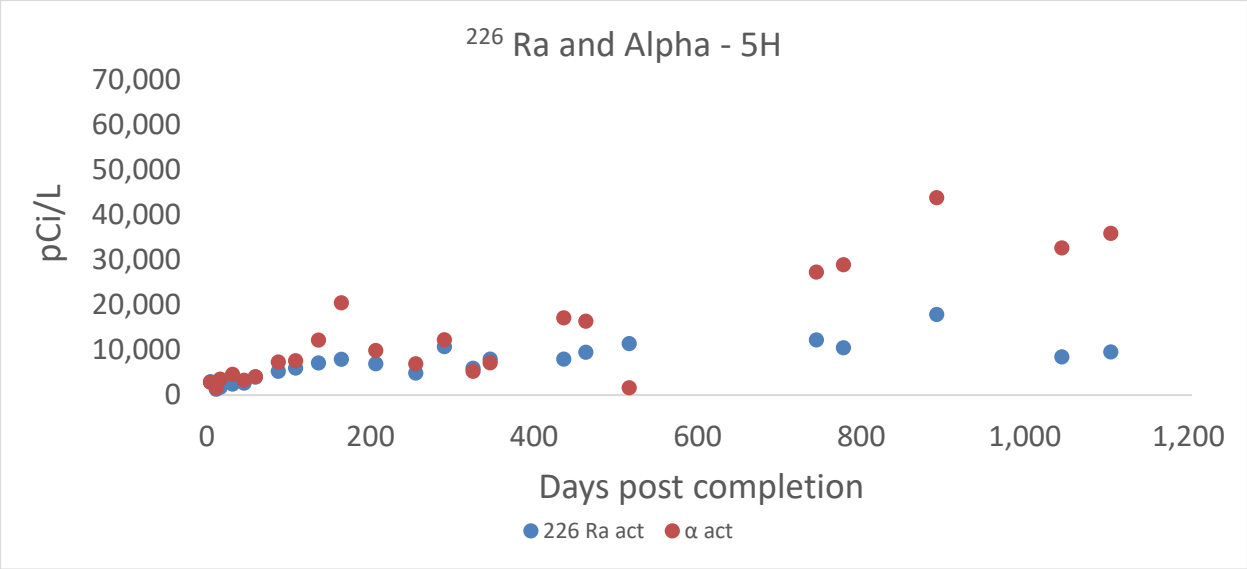

Figure 4.7: The relationship between gross alpha and ^{226}Ra as a function of time post completion at 5H.

The highest values reported in the older wells at 4H and 6H were 15,080 pCi/L gross alpha and 8,078 pCi/L ^{226}Ra. The relationship between gross alpha and ^{226}Ra for wells 4H and 6H are shown in Figure 4.8 and 4.10.

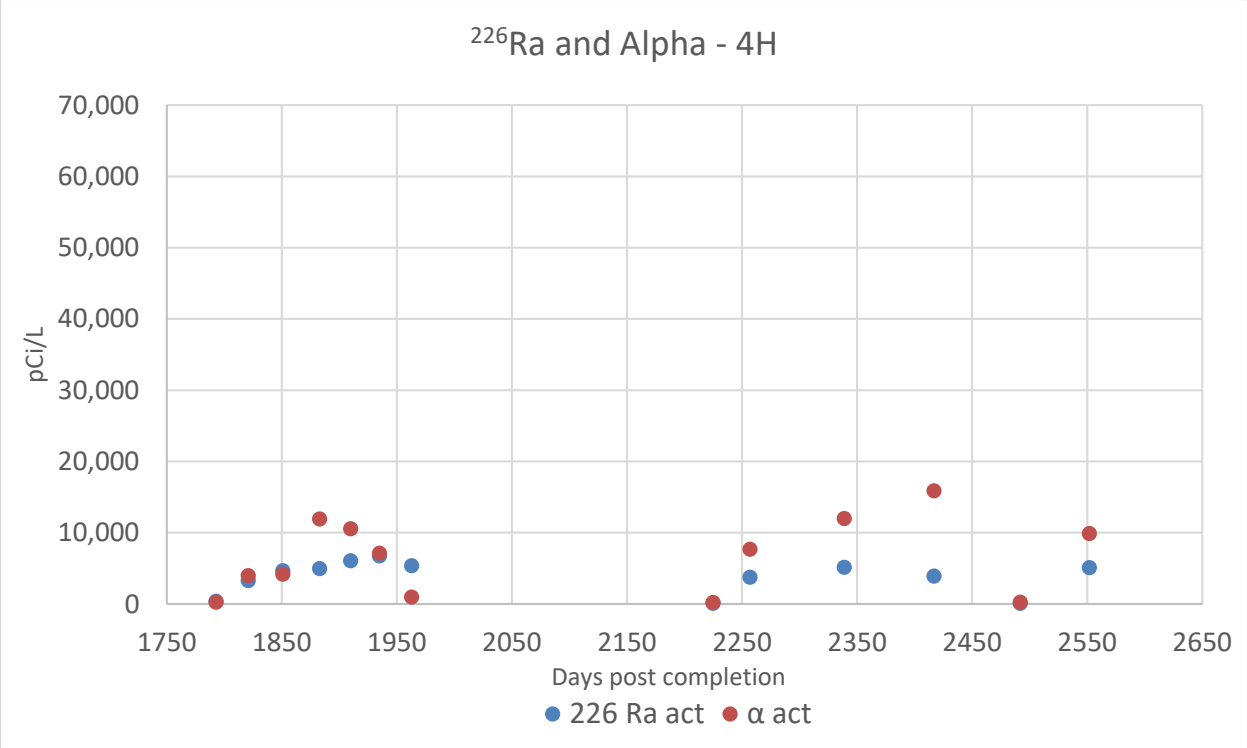

Figure 4.8: The relationship between gross alpha and ^{226}Ra as a function of time post completion at 4H.

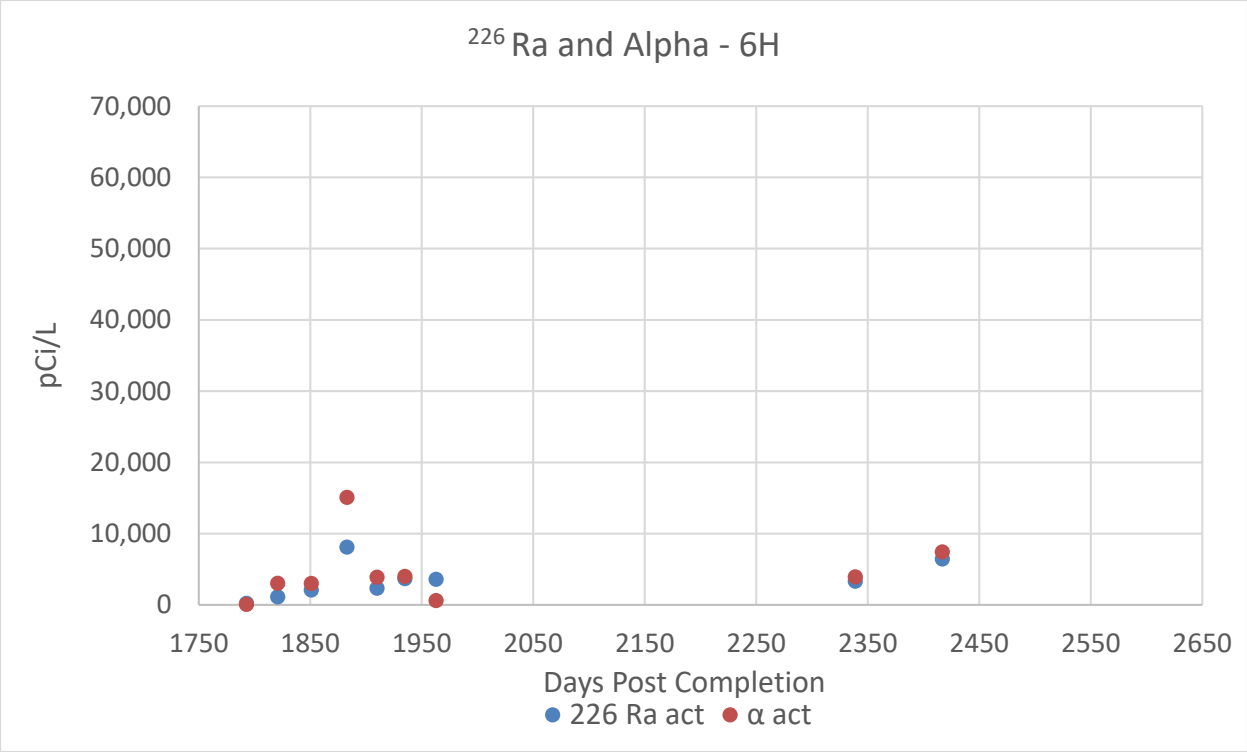

Figure 4.9: The relationship between gross alpha and ^{226}Ra as a function of time post completion at 6H.

Products

N/A for this quarter.

Plan for Next Quarter

The team will continue monthly sampling and analyze flowback/produced water (FPW) from MIP 3H, 4H, 5H and 6H if they are online.

Topic 5 – Environmental Monitoring: Air & Vehicular

Approach

During this quarter the team at WVU completed their 8th audit of the MSEEL site (meeting the milestone). In addition, they continue to develop indirect methane monitoring and quantification methods as part of the additional NSF project occurring at MSEEL 1.0. As a part of this additional research, they will be deploying the mobile system to assess OTM33A indirect style measurements and longer-term eddy co-variance methods from long term deployment of the sensors on the telephone pole mentioned before. Researchers have obtained all of the additional sensors and they have been integrated into the current data collection systems and deployed at MSEEL during the 8th audit. Figure 5.1 shows the new mobile system.

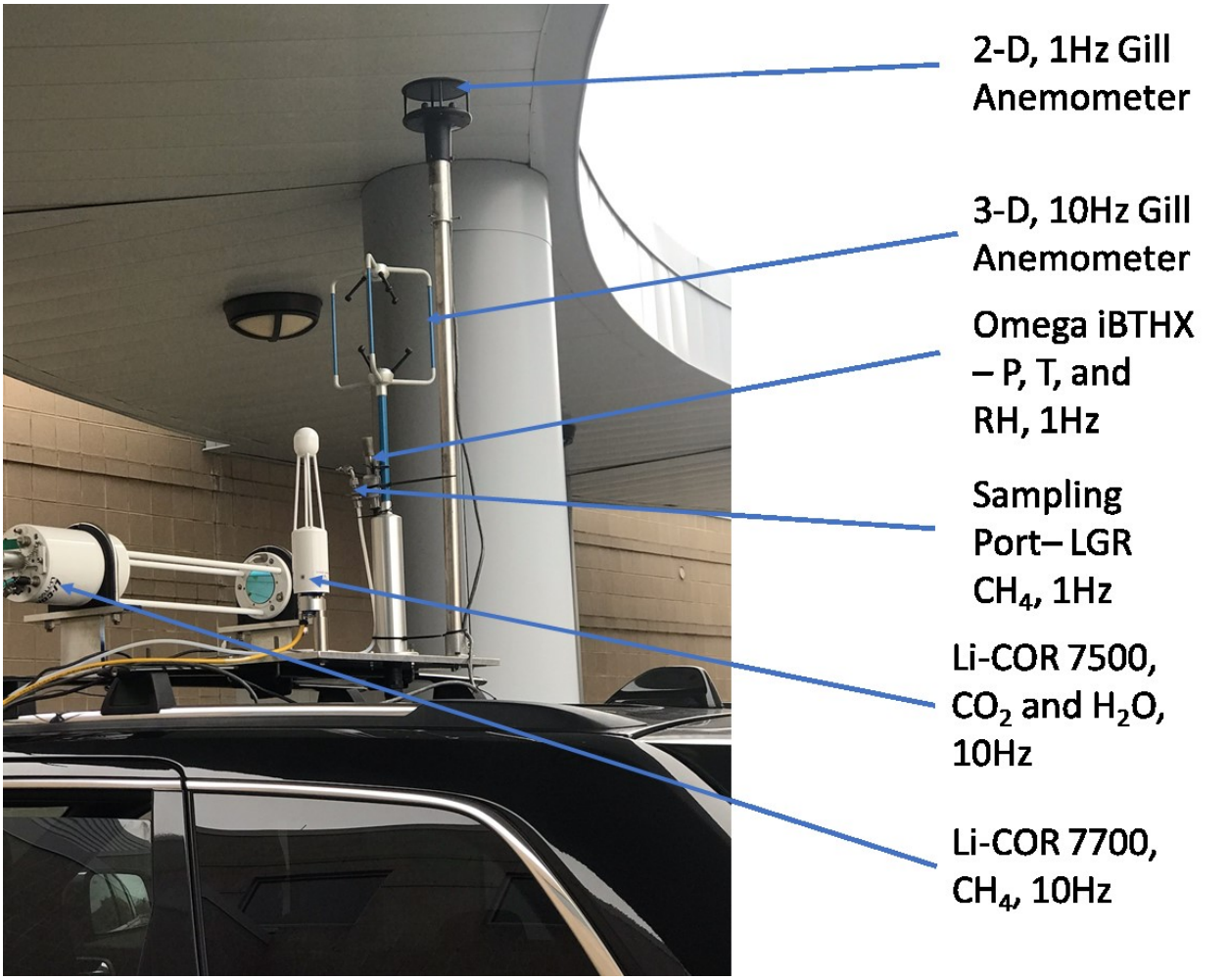

Figure 5.1: Updated mobile system including new Li-COR 7500.

In preparation for the long-term deployment of a stand-alone system for the additional NSF project a stand-alone solar powered data collection system was designed and all equipment except for a transport trailer have been procured. The following list includes the equipment purchased as part of the NSF project for stand-alone data collection efforts for the eddy-covariance system at MSEEL 1.0. It is estimated the system will be capable of operating up to 2-4 days without any appreciable sunlight. The installment has been approved by NNE but researchers are awaiting a transportation trailer that will be used for initial controlled methane releases offsite. A brief summary of the Audit results is presented in the Results and Discussion section.

Components for Eddy-Covariance:

- LI-7500 DS
- Tripod
- Modem
- Solar system
- Mounting kits
- 2 x LG 360 Watt panels
- Tamarack panel mounts
- Charge controllers
- Breakers, cabling, grounding equipment

- Battery enclosure
- 3 x Concorde 210 amp-hour batteries

Results & Discussion

Direct Quantification

The seventh and eighth site audits was completed in October and December 2018. Based on estimated continuation we have made a very tentative schedule for additional audits in the next BP. These are spaced to ensure we have sampled the location at least once in every different month.

Tentative Methane Audit Schedule – MSEEL 1.0

- Audit 9 - February 2019
- Audit 10 - April 2019
- Audit 11 - June 2019
- Audit 12 - September 2019
- Audit 13 - January 2020
- Audit 14 - March 2020
- Audit 15 - May 2020
- Audit 16 - August 2020

Table 5.1 presents the new results as compared with the previous Year 3 audits. Figure 5.2 also presents a column chart with these data as compared to the current MSEEL average and the average of well sites presented in Rella et al. The results of the previous six audits aligned well with trends reported in literature (average of 1371). However, during the last two audits our data were skewed much higher due to excessive tank emissions. In discussions with the operator, one of the EPGUs were replaced meaning that its wells were shut in for the installation that occurred between Audits 6 and 7. However, tank emissions are still high in Audit 8 and the research team is working to determine if the excessive emissions are atypical and due to a stuck dump valve.

Table 5.1: Year 3 and New Year 4 Audits Results.

Component	CH_4 Loss Rate (g/hr)							
	Audit 1	Audit 2	Audit 3	Audit 4	Audit 5	Audit 6	Audit 7	Audit 8
Wellheads	0.85	138	1.64	1.68	5.82	0.68	47.6	32.7
EGPU	356	69.9	58.9	188	200	70.9	N/A	227
Water Tank	84.0	3731	17.3	1032	1074	22.5	43,322	7347
Other	228	163.1	8.43	546	215	11.8	69.4	71.2
Total	669	4102	86.2	1768	1496	106	43,439	7677

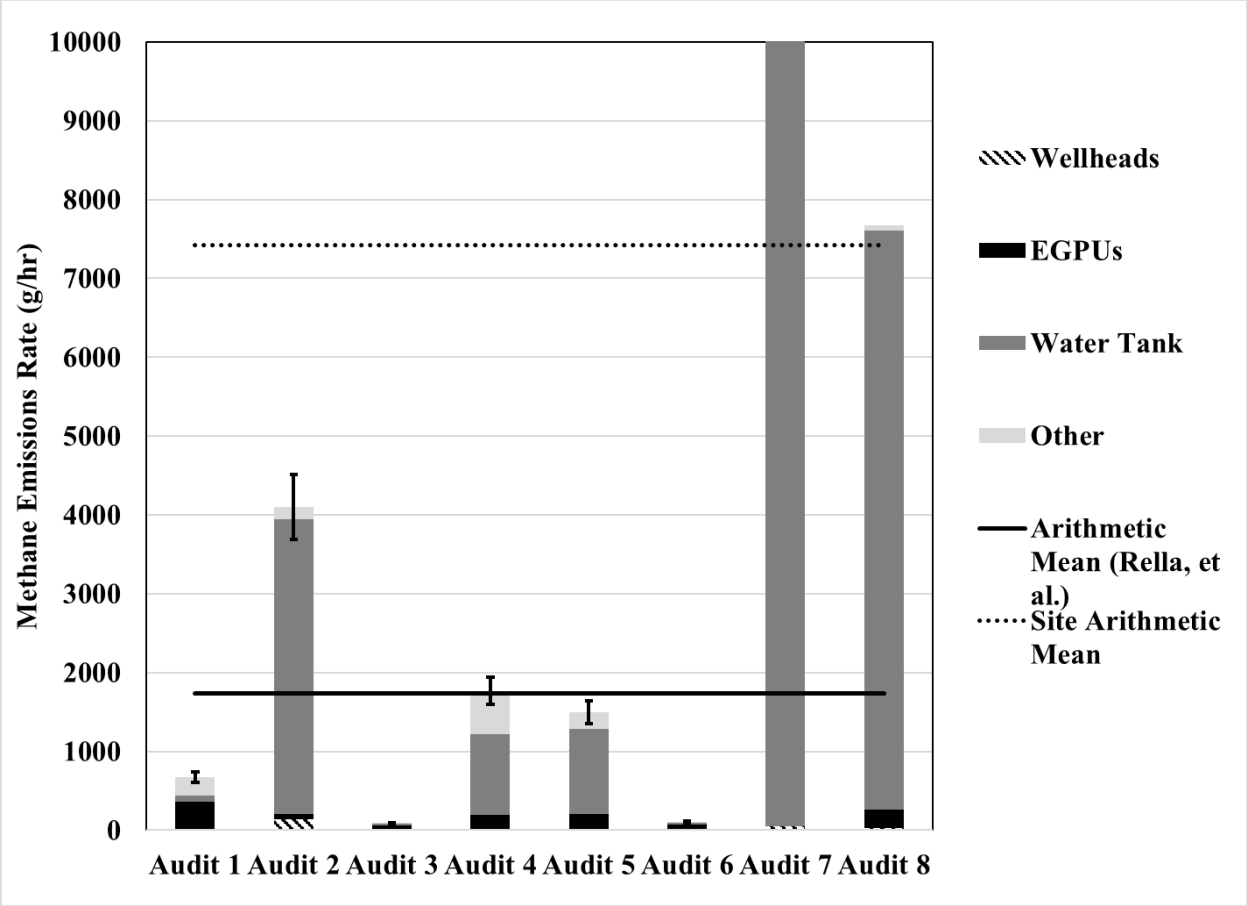

Figure 5.2: Audit Results by Major Source Category (Audits 1-8).

Indirect Monitoring

Figure 5.3 shows two locations (A, B) of the fast sampling system during the deployment during the eighth audit. The general wind direction was from left to right. The north direction "N" faced into the wind. Note that alignments and wind directions have not been refined. Instead of focusing on true upwind and downwind measurements, the team deployed the system at these locations to begin to understand where long term measurements should be focused.

Figure 5.3 General layout during initial deployment of the fast response mobile monitoring system.

Figure 5.4 shows the initial results for wind direction and methane concentration enhancements from the location A. An average background measurement was used to estimate enhancements. The figure shows that most upwind enhancements were 9 to 13 ppm. Figure 5.5 shows the enhancements at location B and they ranged from 3 to 12 ppm. We note that our direct quantification yielded higher mass emissions which likely contributed to higher methane concentrations. Researchers will analyze these data with atmospheric conditions to assess further measurement locations.

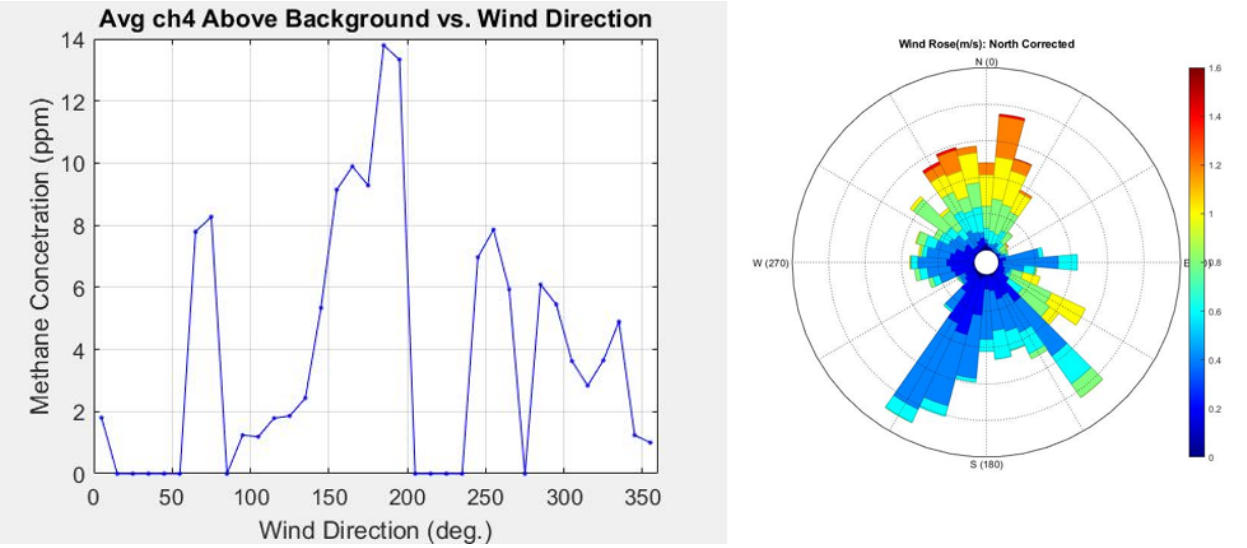

Figure 5.4 Data collected at location A.

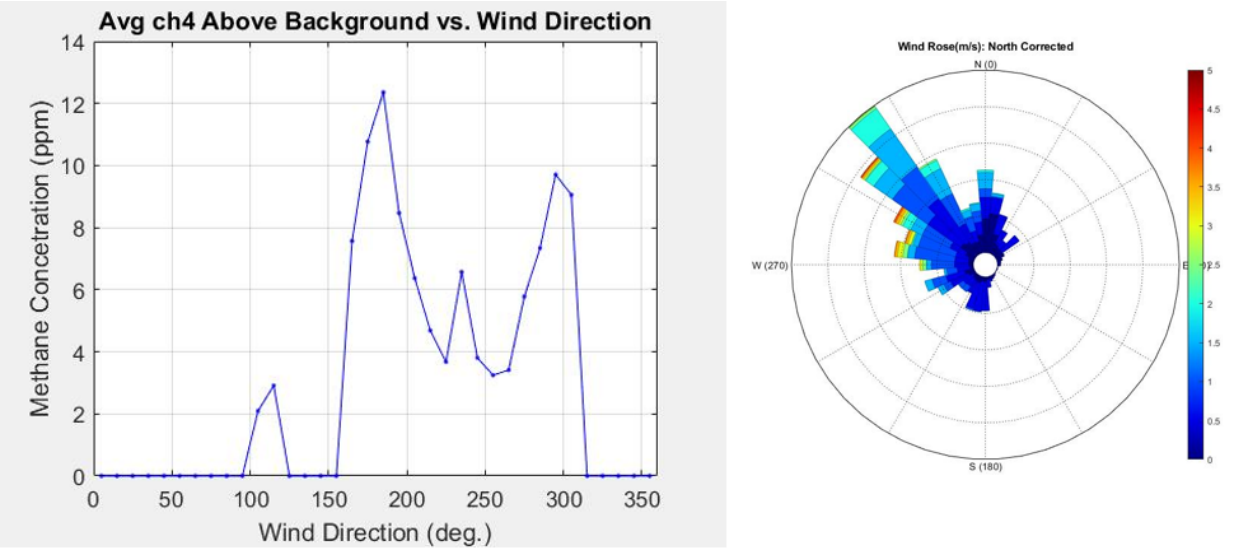

Figure 5.5: Data collected at location B.

Products

A journal article summarizing the results from the initial six audits has been reviewed twice by ACS OMEGA and will likely be published in the following quarter.

Plan for Next Quarter

- Complete Audit 9
- Complete integration of mobile/eddy-covariance system
- Begin installing system at MSEEL 1.0
- Obtain trailer on NSF project to conduct remote controlled methane releases

Topic 6 – Water Treatment

Approach

As part of this subtask, the Dr. Morrissey is characterizing the chemical and biological factors that influence radium accumulation in sludge from produced water. This research could lead to the development of low cost treatments for produced water that prevent the accumulation or radioactive sludge. This work is in service of Milestone 33: *Results of techniques for low cost treatment of flowback waters*. To accomplish this milestone, the team is performing a series of laboratory microcosm experiments. Produced water is incubated for 21 days in the laboratory with or without additions of sulfate (2000mg/L) and nutrients (carbon, nitrogen and phosphorus). The addition of nutrients is intended to stimulate the activity of microorganisms to immobilize sulfate and prevent it from precipitating with radium. Tests thus far have utilized produced water from the 3H.

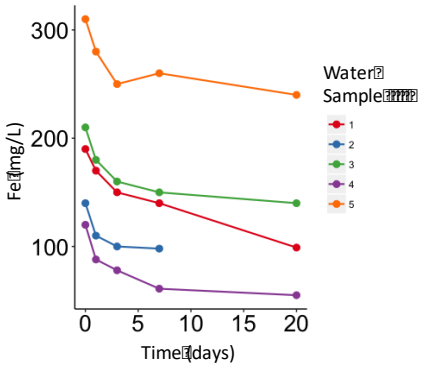

Figure 6.1: Iron concentration over time during storage of five independently collected produced water samples from well 3H.

Results & Discussion

Milestone 1) Characterize chemical transformations during produced water storage from well 3H. Morrissey's team will complete characterization of changes in produced water chemistry (specifically Fe, Sr, Ba, Ra 226, Ra 228) and biological activity (CO_2 and CH_4 production) that occur during short term storage (20 days). Measure Ra activity (Ra 226 and Ra 228) of solid precipitate formed during short term storage of produced water. An analysis will be completed on a minimum of 5 independently collected produced water samples collected between December 2017 and January 2019.

Results for Milestone 1

Table 6.1: Concentration of select cations in produced water from well 3H.

	Sr (mg/L)	Ba (mg/L)	^{226}Ra (pCi/L)	^{228}Ra (pCi/L)
Mean	1918	4204	13839	800.7
Min	522	1160	3691	181.3
Max	3140	7020	20903	1244.5

Analysis of five independently collected water samples gathered between December 2017 and August 2018 revealed high variation in water chemistry. The concentrations of important scale forming cations (e.g. Ba and Sr) as well as Ra did not change over time (Table 6.1). Similarly, concentrations of Na, Ca, and Cl were stable over time. Sulfate concentrations were always below detection. The only ion that changed over the 20-day incubation was Fe, which decreased ~70 mg/L on average. A relatively small amount of Ra precipitated over the 20-day incubation, 31.4 pg ^{226}Ra/L on average (range 8.8 -76.6 pg ^{226}Ra/L). Biological activity, as estimated by CO_2 and CH_4 production, also varied among samples (Figure 6.2). Rates of methane production were highest immediately after sampling and declined over

the 20-day incubation. In general CO_2 production rates were ten fold higher than CH_4 production rates.

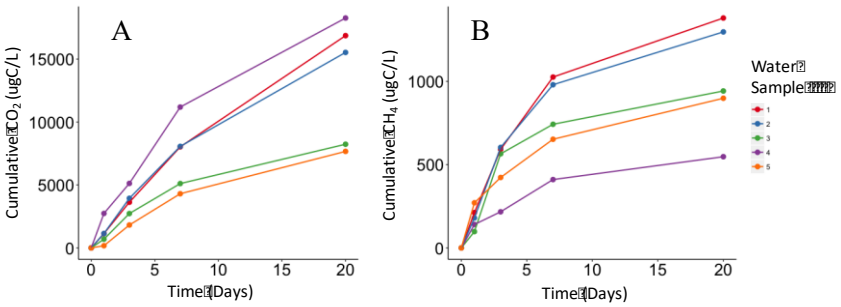

Figure 6.2: Cumulative production of CO_2 (A) and CH_4 (B) from five independently collected produced water samples.

Milestone 2. Document effects of sulfate and nutrient additions on chemical transformations during produced water storage from well 3H. We will characterize the effect of sulfate and nutrient additions on changes in produced water chemistry (specifically Fe, Sr, Ba, Ra 226, Ra 228) and biological activity (CO_2 and CH_4 production) during short term storage (20 days). Effects on Ra activity (Ra 226 and Ra 228) of solid precipitate formed will also be measured. We expect to complete these analyses on a minimum of 3 independently collected produced water samples collected between December 2017 and January 2019.

Results for Milestone 2

Sulfate and nutrient additions were added to three independently collected water samples gathered between January and August 2018. Nutrient additions had no detectable impact on water chemistry dynamics but did increase CO_2 production rates. The amount of 226Ra in solid precipitate slight increased with nutrient additions averaging 331 pg/L (range 263-425 pg/L). Sulfate addition caused a near immediate drop in the concentration of Ba (Figure 6.3A). The chemistry suggests that one mole of sulfate precipitates ~0.8 moles of Ba. When Ba precipitates Ra concentrations decrease proportionally (Figure 6.3B). Consequently, SO_4 caused Ra to

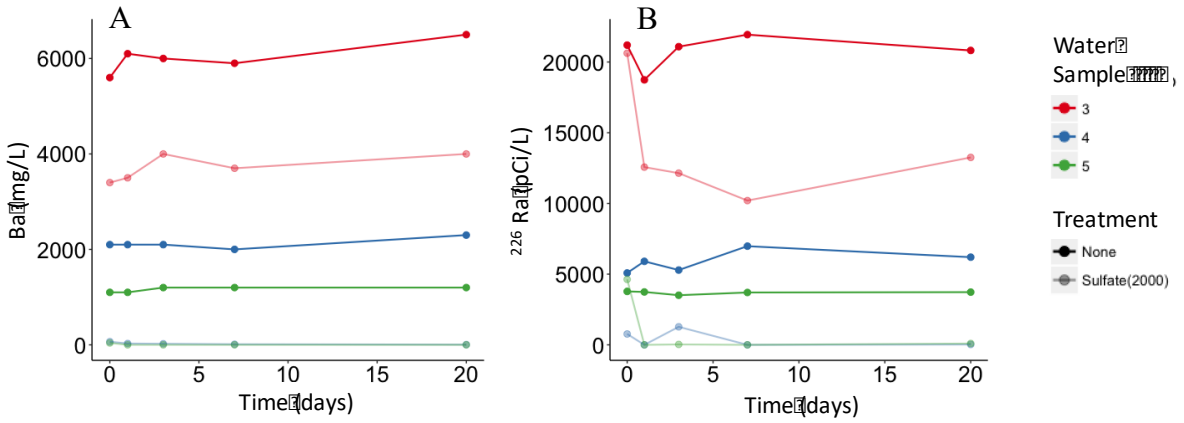

Figure 6.3: Changes in Ba (A) and 226 Ra (B) due to the addition of SO_4. Data is shown for three independently collected water samples indicated by color, samples amended with SO_4 are shown in a lighter shade.

accumulate in the solid precipitate in proportion to its original concentration in the produced water sample (Figure 6.4). Our data suggests Ra can be removed by SO_4 addition via co-precipitation with Ba.

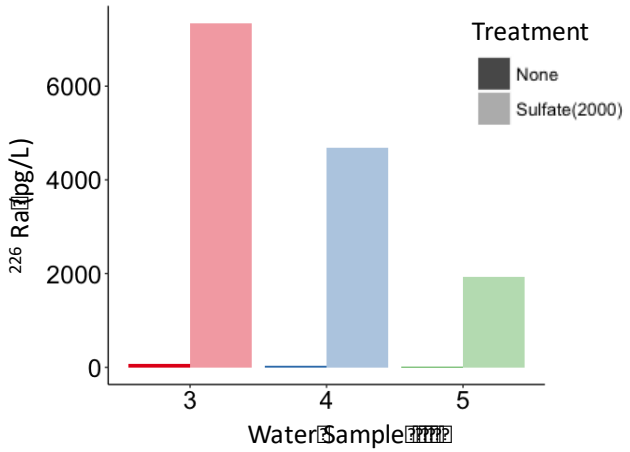

Figure 6.4: Mass of ^{226}Ra in solid precipitate per liter of produced water in three untreated (dark shade) and sulfate amended (light shade) water samples from well 3H (indicated by color).

Products

Pending sample analysis, the team will submit this work for publication.

Plan for Next Quarter

In the next quarter Dr. Morrissey will examine the microbial communities within these samples and continue data analysis.

Topic 7 – Database Development

Approach

All MSEEL data is now online and available to researchers (Figure 7.1 and 7.2). The website has been updated with the latest production beyond the end of the quarter (Figure 7.3). Work continues

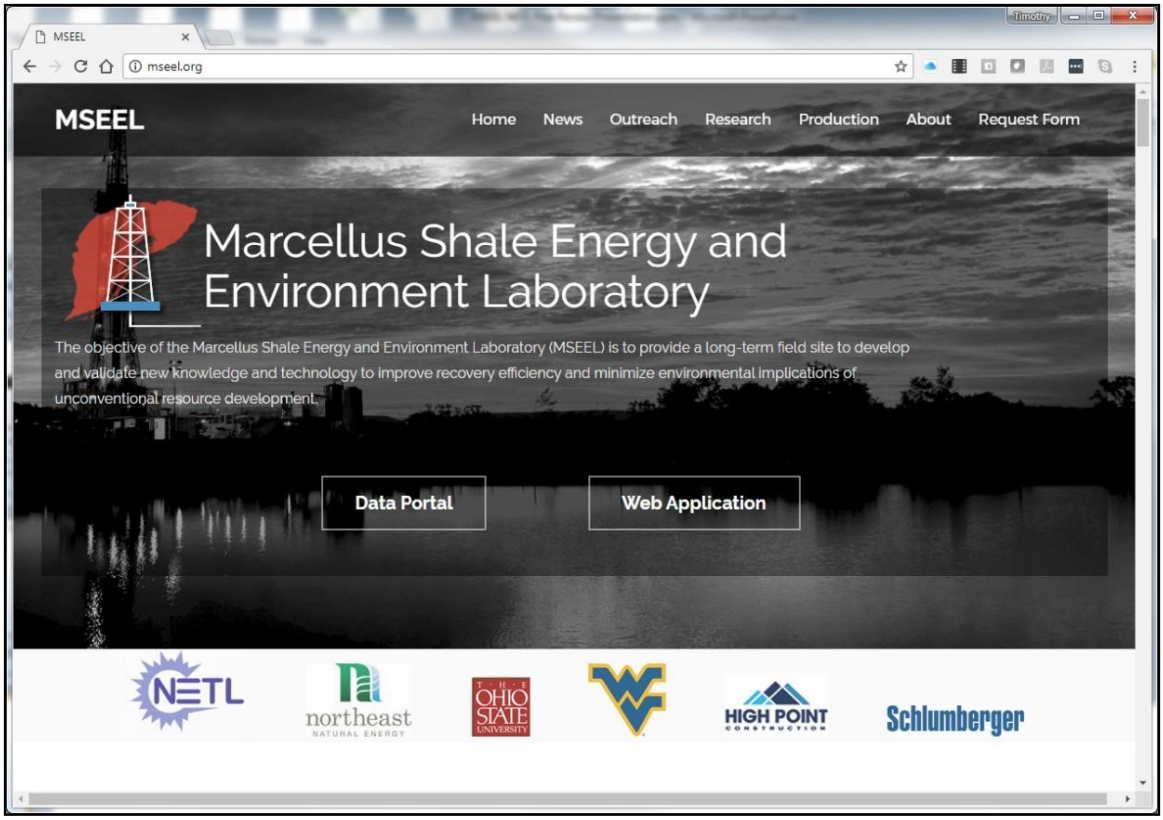

Figure 7.1: MSEEL website at http://mseel.org/.

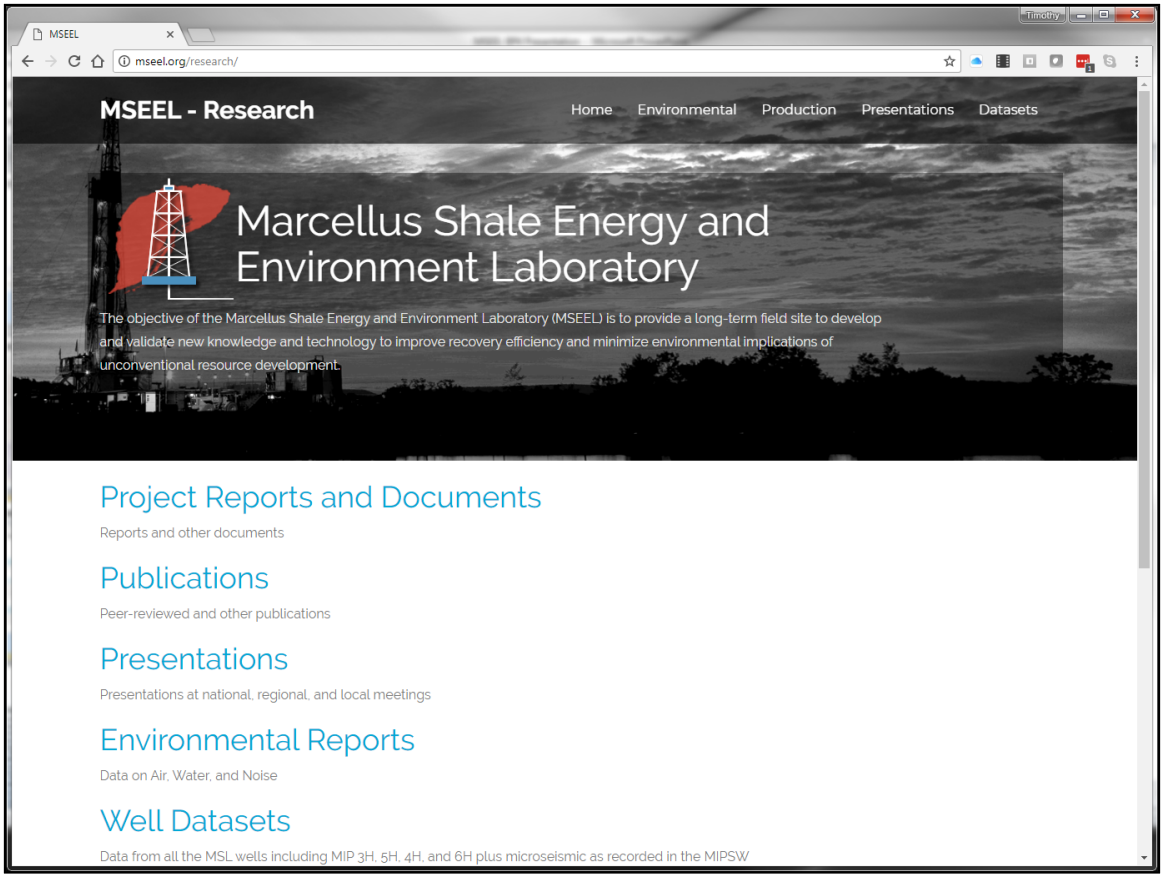

Figure 7.2: All data generated by the MSEEL project is available for download at http://mseel.org/.

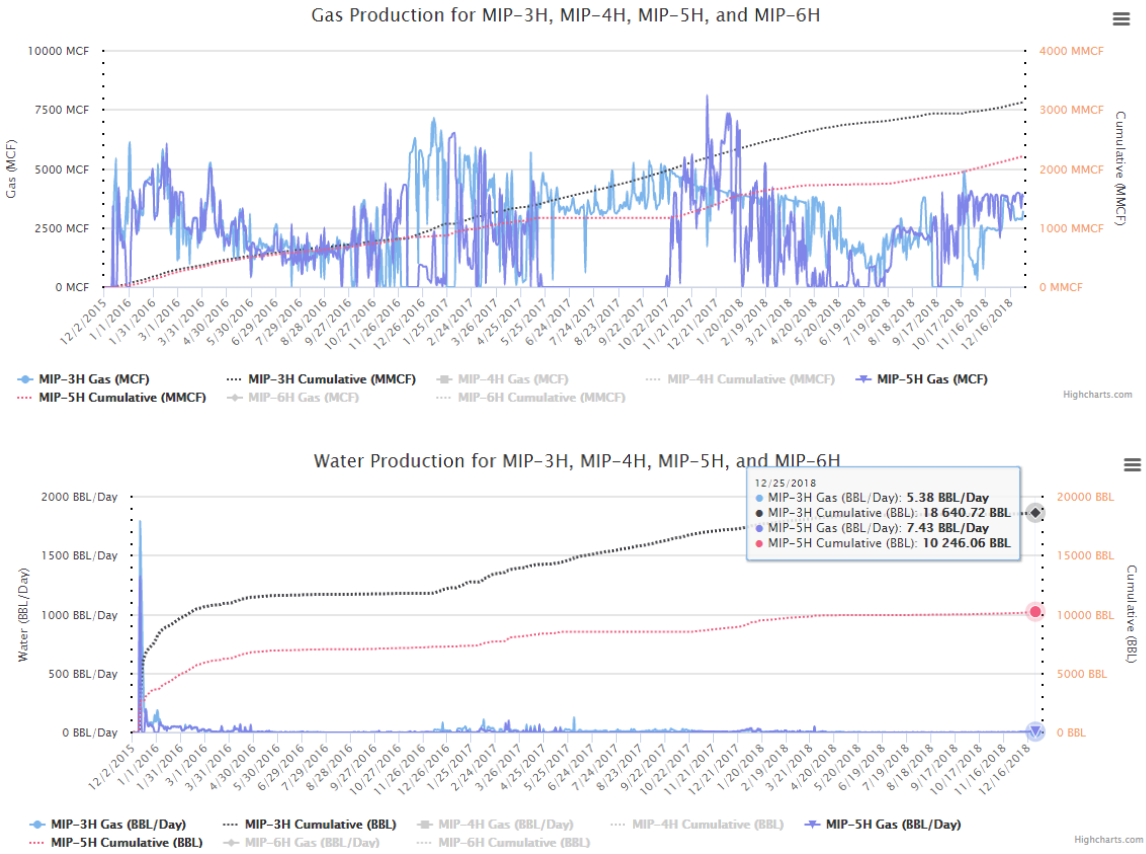

Figure 7.3: Gas and water production have been updated through the end of the quarter and are available at http://mseel.org/.

Results & Discussion

Data and publications are now available at http://mseel.org/.

Products

Web site enhanced and updated.

Plan for Next Quarter

Working to develop interactive programs to display user selected well logs and geochemical data. A mock-up of the type of display is shown in Figure 7.4.

Topic 8 – Economic and Societal

This task is complete and will not be updated in future reports.

Cost Status

Year 1

Start: 10/01/2014 End: 09/30/2017

Baseline Reporting Quarter

	Q1 (12/31/14)	Q2 (3/30/15)	Q3 (6/30/15)	Q4 (9/30/15)
Baseline Cost Plan	(From 424A, Sec. D)			
(from SF-424A)				
Federal Share	$549,000		$3,549,000	
Non-Federal Share	$0.00		$0.00	
Total Planned (Federal and Non-Federal)	$549,000		$3,549,000	
Cumulative Baseline Costs				
Actual Incurred Costs				
Federal Share	$0.00	$14,760.39	$237,451.36	$300,925.66
Non-Federal Share	$0.00	$0.00	$0.00	$0.00
Total Incurred Costs - Quarterly (Federal and Non-Federal)	$0.00	$14,760.39	$237,451.36	$300,925.66
Cumulative Incurred Costs	$0.00	$14,760.39	$252,211.75	$553,137.41
Uncosted				
Federal Share	$549,000	$534,239.61	$3,296,788.25	$2,995,862.59
Non-Federal Share	$0.00	$0.00	$2,814,930.00	$2,814,930.00
Total Uncosted - Quarterly (Federal and Non-Federal)	$549,000	$534,239.61	$6,111,718.25	$5,810,792.59

Start: 10/01/2014 End: 09/30/2017

Baseline Reporting Quarter

	Q5 (12/31/15)	Q6 (3/30/16)	Q7 (6/30/16)	Q8 (9/30/16)
Baseline Cost Plan	(From 424A, Sec. D)			
(from SF-424A)				
Federal Share	$6,247,367		$7,297,926	
Non-Federal Share	2,814,930		$4,342,480	
Total Planned (Federal and Non-Federal)	$9,062,297	$9,062,297.00	$11,640,406	
Cumulative Baseline Costs				
Actual Incurred Costs				
Federal Share	$577,065.91	$4,480,939.42	$845,967.23	$556,511.68
Non-Federal Share	$0.00	$2,189,863.30	$2,154,120.23	$0.00
Total Incurred Costs - Quarterly (Federal and Non-Federal)	$577,065.91	$6,670,802.72	$3,000,087.46	$556,551.68
Cumulative Incurred Costs	$1,130,203.32	$7,801,006.04	$10,637,732.23	$11,194,243.91
Uncosted				
Federal Share	$5,117,163.68	$636,224.26	$1,004,177.30	$447,665.62
Non-Federal Share	$2,814,930.00	$625,066.70	($1,503.53)	($1,503.53)
Total Uncosted - Quarterly (Federal and Non-Federal)	$2,418,796.68	$1,261,290.96	$1,002,673.77	$446,162.09

Start: 10/01/2014 End: 09/30/2017

Baseline Reporting Quarter	Q9 (12/31/16)	Q10 (3/30/17)	Q11 (6/30/17)	Q12 (9/30/17)
Baseline Cost Plan	(From 424A, Sec. D)			
(from SF-424A)				
Federal Share				$9,128,731
Non-Federal Share				$4,520,922
Total Planned (Federal and Non-Federal)				$13,649,653
Cumulative Baseline Costs				
Actual Incurred Costs				
Federal Share	$113,223.71	$196,266.36	$120,801.19	$1,147,988.73
Non-Federal Share	$0.00	$0.00	$0.00	$0.00
Total Incurred Costs - Quarterly (Federal and Non-Federal)	$113,223.71	$196,266.36	$120,801.19	$1,147,988.73
Cumulative Incurred Costs	$11,307,467.62	$11,503,733.98	$11,624535.17	$12,772,523.90
Uncosted				
Federal Share	$334,441.91	$138,175.55	$17,374.36	$700,190.63
Non-Federal Share	($1,503.53)	($1,503.53)	($1,503.53)	$176,938.47
Total Uncosted - Quarterly (Federal and Non-Federal)	$332,938.38	$136,672.02	$15,870.83	$877,129.10

Start: 10/01/2014 End: 09/30/2017

Baseline Reporting Quarter	Q13 (12/31/17)	Q14 (3/30/18)	Q15 (6/30/18)	Q15 (9/30/18)
Baseline Cost Plan	(From 424A, Sec. D)			
(from SF-424A)				
Federal Share				$11,794,054
Non-Federal Share				$5,222,242
Total Planned (Federal and Non-Federal)				$17,016,296.00
Cumulative Baseline Costs				
Actual Incurred Costs				
Federal Share	$112,075.89	$349,908.08	$182,207.84	$120,550.20
Non-Federal Share	$0.00	$31,500.23	$10,262.40	$4,338.00
Total Incurred Costs - Quarterly (Federal and Non-Federal)	$112,075.89	$381,408.31	$192,470.24	$124,888.20
Cumulative Incurred Costs	$12,884,599.79	$13,266,008.10	$13,458,478.34	$13,583,366.54
Uncosted				
Federal Share	$588,114.74	$238,206.66	$55,998.82	$2,600,771.62
Non-Federal Share	$176,938.47	$145,438.24	$135,175.84	$832,157.84
Total Uncosted - Quarterly (Federal and Non-Federal)	$765,053.21	$383,644.90	$191,174.66	$3,432,929.46

Start: 10/01/2014 End: 03/31/2019

Baseline Reporting Quarter	Q17 (12/31/18)	Q18 (3/30/19)	Q19 (6/30/19)	Q20 (9/30/19)
Baseline Cost Plan	(From 424A, Sec. D)			
(from SF-424A)				
Federal Share				
Non-Federal Share				
Total Planned (Federal and Non-Federal)				
Cumulative Baseline Costs				
Actual Incurred Costs				
Federal Share	$80,800.03			
Non-Federal Share	$4,805.05			
Total Incurred Costs - Quarterly (Federal and Non-Federal)	$85,605.08			
Cumulative Incurred Costs	$13,668,971.62			
Uncosted				
Federal Share	$2,519,971.59			
Non-Federal Share	$827,352.79			
Total Uncosted - Quarterly (Federal and Non-Federal)	$3,347,324.38			

National Energy Technology Laboratory

626 Cochrans Mill Road
P.O. Box 10940
Pittsburgh, PA 15236-0940

3610 Collins Ferry Road
P.O. Box 880
Morgantown, WV 26507-0880

13131 Dairy Ashford Road, Suite 225
Sugar Land, TX 77478

1450 Queen Avenue SW
Albany, OR 97321-2198

Arctic Energy Office
420 L Street, Suite 305
Anchorage, AK 99501

Visit the NETL website at:
www.netl.doe.gov

Customer Service Line:
1-800-553-7681